A rivulet of perfectly wetting fluid draining steadily down a slowly varying substrate

S. K. Wilson[1] and B. R. Duffy[2]

Department of Mathematics,
University of Strathclyde,
Livingstone Tower,
26 Richmond Street,
Glasgow G1 1XH,
United Kingdom

Running Title : A rivulet of perfectly wetting fluid

10th January 2003, revised 3rd November 2003

---

[1]Author for correspondence. Telephone : + 44 (0)141 548 3820, Fax : + 44 (0)141 552 8657, Email : s.k.wilson@strath.ac.uk

[2]Telephone : + 44 (0)141 548 3645, Fax : + 44 (0)141 552 8657, Email : b.r.duffy@strath.ac.uk

Abstract

We use the lubrication approximation to investigate the steady locally unidirectional gravity-driven draining of a thin rivulet of a perfectly wetting Newtonian fluid with prescribed volume flux down both a locally planar and a locally non-planar slowly varying substrate inclined at an angle α to the horizontal. We interpret our results as describing a slowly varying rivulet draining in the azimuthal direction some or all of the way from the top ($\alpha = 0$) to the bottom ($\alpha = \pi$) of a large horizontal circular cylinder with a non-uniform transverse profile. In particular, we show that the behaviour of a rivulet of perfectly wetting fluid is qualitatively different from that of a rivulet of a non-perfectly wetting fluid.

In the case of a locally planar substrate we find that there are no rivulets possible in $0 \le \alpha \le \pi/2$ (i.e. there are no sessile rivulets or rivulets on a vertical substrate), but that there are infinitely many pendent rivulets running continuously from $\alpha = \pi/2$ (where they become infinitely wide and vanishingly thin) to $\alpha = \pi$ (where they become infinitely deep with finite semi-width).

In the case of a locally non-planar substrate with a power-law transverse profile with exponent $p > 0$ we find, rather unexpectedly, that the behaviour of the possible rivulets is qualitatively different in the cases $p < 2$, $p = 2$ and $p > 2$ as well as in the cases of locally concave and locally convex substrates. In the case of a locally concave substrate there is always a solution near the top of the cylinder representing a rivulet that becomes infinitely wide and deep, whereas in the case of a locally convex substrate there is always a solution near the bottom of the cylinder representing a rivulet that becomes infinitely deep with finite semi-width. In both cases the extent of the rivulet around the cylinder and its qualitative behaviour depend on the value of p. In the special case $p = 2$ the solution represents a rivulet on a locally parabolic substrate that becomes infinitely wide and vanishingly thin in the limit $\alpha \to \pi/2$. We also determine the behaviour of the solutions in the physically important limits of a weakly non-planar substrate, a strongly concave substrate, a strongly convex substrate, a small volume flux, and a large volume flux.

2

1 Introduction

Gravity-driven rivulet flows occur in a wide variety of practical situations ranging from industrial situations such as coating processes and heat exchangers to geophysical situations such as mud and lava flows. As a result of their numerous practical occurrences there has been considerable theoretical work on a variety of rivulet flows in recent years, much of it building on the pioneering analysis of the steady unidirectional flow of a Newtonian fluid down an inclined plane in the presence of significant surface-tension effects by Towell & Rothfeld (1966). In particular, Allen & Biggin (1974) and subsequently Duffy & Moffatt (1995) used the lubrication approximation to obtain the leading-order solution in the asymptotic limit in which the aspect ratio of the transverse cross-sectional profile of the rivulet is small, i.e. in which the transverse profile of the rivulet is thin. Specifically Duffy & Moffatt (1995) calculated the shape of the rivulet as a function of α, the angle of inclination of the substrate to the horizontal, and interpreted their results as describing the locally unidirectional flow down a locally planar substrate whose local slope α varies slowly in the flow-wise direction and, in particular, used them to describe the flow in the azimuthal direction round a large horizontal circular cylinder. Subsequently Wilson & Duffy (1998) extended this analysis to study the locally unidirectional flow of a rivulet down a locally non-planar slowly varying substrate. In particular, they found that a rivulet can run continuously from the top to the bottom of a large horizontal circular cylinder with a trough or ridge in the azimuthal direction only if the transverse profile of the substrate is that of a sufficiently shallow trough; if the profile is a deeper trough then no such rivulet is possible near the bottom of the cylinder, while if the profile is a ridge then no such rivulet is possible near the top of the cylinder. More generally, various aspects of free-surface flow with significant surface-tension effects down an open channel were considered by Kuo & Tanner (1972) and Hansen & Solonnikov (1990). The important but difficult problem of the

3

stability of rivulet flow has been investigated by Davis (1980), Weiland & Davis (1981), Young & Davis (1987), Schmuki & Laso (1990) and Wilson & Duffy (1998).

All of the work described above is concerned with rivulets of a fluid that *wets the substrate non-perfectly*, i.e. with rivulets that have a *non-zero contact angle* at their contact lines with the substrate. Rather surprisingly there has been almost no work on rivulets of a fluid that *wets the substrate perfectly*, i.e. on rivulets that have a *zero contact angle*. Very recently Duffy & Wilson (2003) have analysed the locally unidirectional flow of a rivulet of perfectly wetting fluid with temperature-dependent viscosity down a uniformly heated or cooled slowly varying substrate. The only other work on rivulet flow of a perfectly wetting fluid of which the authors are aware is that by Kuibin (1996) and Alekseenko, Geshev & Kuibin (1997) who considered unidirectional flow on the underside of a circular pipe. In particular, Kuibin (1996) obtained the leading-order asymptotic solution for a narrow rivulet of a perfectly wetting fluid on the underside of a locally parabolic substrate.

In the present paper we shall use the lubrication approximation to investigate the steady locally unidirectional gravity-driven draining of a thin rivulet of a perfectly wetting Newtonian fluid with prescribed volume flux down both a locally planar and a locally non-planar slowly varying substrate. In particular, we shall show that the behaviour of a rivulet of perfectly wetting fluid is *qualitatively different* from that of a rivulet of a non-perfectly wetting fluid described by Duffy & Moffatt (1995) and Wilson & Duffy (1998). Specifically we shall consider the case of a substrate whose local transverse profile is that of a power law in the transverse coordinate with exponent $p > 0$, and we shall find, rather unexpectedly, that the behaviour of the possible rivulets is *qualitatively different* in the cases $p < 2$, $p = 2$ and $p > 2$ as well as in the cases of locally concave and locally convex substrates. Kuibin's (1996) solution will be recovered as a limiting case of the present results in the special case $p = 2$.

4

2 Problem Formulation

Consider initially the steady unidirectional gravity-driven draining of a thin symmetric rivulet of constant (but unknown) semi-width a of perfectly wetting Newtonian fluid with prescribed positive volume flux $Q = \bar{Q} > 0$ down a symmetric substrate inclined at an angle α ($0 \leq \alpha \leq \pi$) to the horizontal. Following the approach of Wilson & Duffy (1998) in the non-perfectly wetting case we consider a non-planar substrate whose profile varies transversely to the direction of flow but not in the direction of flow. We choose Cartesian axes $Oxyz$ as indicated in Fig. 1, with the x axis in the direction of flow and the y axis horizontal (transverse to the direction of flow) with respect to which the (known) position of the substrate is denoted by $z = H(y)$ and the (unknown) position of the free surface by $z = (H + h)(y)$, where $h = h(y) \geq 0$ denotes the (unknown) thickness of the rivulet. The velocity $\mathbf{u} = u(y, z)\mathbf{i}$ and pressure $p = p(x, y, z)$ of the fluid are governed by the familiar mass-conservation and Navier–Stokes equations. The fluid is assumed to have constant density ρ, viscosity μ and surface tension γ. On the substrate the fluid velocity is zero, while on the free surface the usual normal and tangential stress balances and the kinematic condition apply. Since the fluid is perfectly wetting, at the edges of the rivulet $y = \pm a$ where $h = 0$ the contact angle takes the prescribed value of zero.

Analytical progress can be made by considering the case of a rivulet whose cross section is slender with small aspect ratio $\epsilon \ll 1$, and thus we scale the system appropriately by writing

$$y = ly^*, \quad a = la^*, \quad z = \epsilon l z^*, \quad h = \epsilon l h^*, \quad H = \epsilon l H^*,$$
$$u = \frac{\rho g \epsilon^2 l^2}{\mu} u^*, \quad Q = \frac{\rho g \epsilon^3 l^4}{\mu} Q^*, \quad p = p_\infty + \rho g \epsilon l p^*, \tag{1}$$

where $l = (\gamma/\rho g)^{1/2}$ is the capillary length in which g denotes acceleration due to gravity, and p_∞ is the uniform pressure of the surrounding atmosphere. In the non-perfectly wetting case Wilson & Duffy (1998) identify ϵ with the (non-zero) contact angle. In the perfectly wetting case this choice is not possible and we can adopt one of several alternative definitions of ϵ,

5

including

$$\epsilon = \left(\frac{\rho g \mu \bar{Q}}{\gamma^2} \right)^{1/3} \tag{2}$$

(corresponding to setting $\bar{Q}^* = 1$). However since there are other equally sensible choices we leave ϵ arbitrary in what follows in order to keep the presentation as general as possible. The star subscripts will be dropped immediately for clarity, and hereafter all quantities are non-dimensional unless it is stated otherwise.

The leading-order versions of the components of the governing Navier–Stokes equation are

$$0 = \sin \alpha + u_{zz}, \quad 0 = -p_y, \quad 0 = -p_z - \cos \alpha, \tag{3}$$

to be integrated subject to the boundary conditions of no slip at the substrate $z = H$,

$$u = 0, \tag{4}$$

balances of normal and tangential stress at the free surface $z = H + h$,

$$p = -(H + h)'', \quad u_z = 0, \tag{5}$$

and zero contact angle at the edges of the rivulet $y = \pm a$,

$$h = 0, \quad h' = 0. \tag{6}$$

Primes denote differentiation with respect to argument. Note that the mass-conservation equation and the kinematic condition are satisfied identically.

Integrating (3c) subject to (5a) at $z = H + h$ yields

$$p = (H + h - z) \cos \alpha - (H + h)''. \tag{7}$$

Then (3b) yields a third-order ordinary differential equation for h, namely

$$\left[(H + h)'' - Sm^2(H + h) \right]' = 0, \tag{8}$$

6

where we have introduced the notation $S = \text{sgn}(\cos \alpha)$ and $m = |\cos \alpha|^{1/2}$. Equation (8) is to be integrated subject to (6) at $y = \pm a$. For the solution to be physically realisable h must satisfy $h \geq 0$ for $|y| \leq a$, and so, in particular, it must satisfy $h(0) \geq 0$ and $h''(\pm a) \geq 0$. Integrating (3a) subject to (4) at $z = H$ and (5b) at $z = H + h$ yields

$$u = \frac{\sin \alpha}{2}(z - H)(2h + H - z), \tag{9}$$

and so the local flux $\bar{u} = \bar{u}(y)$ is given by

$$\bar{u} = \int_0^h u \, dz = \frac{\sin \alpha}{3} h^3, \tag{10}$$

and hence the flux of fluid down the rivulet, Q, is given by

$$Q = \int_{-a}^{+a} \bar{u} \, dy = \frac{2 \sin \alpha}{3} \int_0^a h^3 \, dy. \tag{11}$$

So far the analysis has been restricted to strictly unidirectional flow but, as Wilson & Duffy (1998) describe in the non-perfectly wetting case, this solution is also the leading-order approximation to the local behaviour of a rivulet with non-uniform width draining down a non-planar cylindrical substrate, where α now represents the *local* inclination of the substrate to the horizontal, provided that α varies sufficiently slowly, i.e. provided that both the longitudinal aspect ratio and the reduced Reynolds number are sufficiently small. Thus we shall interpret the results given subsequently as describing a slowly varying rivulet draining in the azimuthal direction from the top ($\alpha = 0$) to the bottom ($\alpha = \pi$) of a large horizontal circular cylinder with a non-uniform transverse profile.

3 The Locally Planar Case $H \equiv 0$

In the special case $H \equiv 0$ the substrate is locally planar. Solving (8) subject to (6) at $y = \pm a$ shows that *no* solution is possible when $\cos \alpha \geq 0$ (i.e. for a sessile rivulet or a rivulet on a vertical substrate) but that *infinitely many* solutions are possible when $\cos \alpha < 0$ (i.e. for a

7

pendent rivulet), namely

$$a = \frac{n\pi}{m} \tag{12}$$

and

$$h = \left[\frac{3\bar{Q}m}{5n\pi \sin\alpha} \right]^{1/3} [1 - (-1)^n \cos my] \tag{13}$$

for $n = 1, 2, 3, \ldots$. In particular, these solutions show that the semi-width a (but not the profile h) of the rivulet is, rather surprisingly, *independent* of the value of the flux $\bar{Q}$. For odd values of n the solution for h attains its minimum value of zero $(n+1)/2$ times in $0 \le y \le a$ at $y/a = 1/n, 3/n, \ldots, (n-2)/n, 1$ and its maximum value of

$$h_{\mathrm{m}} = h(0) = 2 \left[\frac{3\bar{Q}m}{5n\pi \sin\alpha} \right]^{1/3} \tag{14}$$

$(n+1)/2$ times in $0 \le y \le a$ at $y/a = 0, 2/n, \ldots, (n-1)/n$. For even values of n the solution for h attains its minimum value of zero $(n+2)/2$ times in $0 \le y \le a$ at $y/a = 0, 2/n, \ldots, (n-2)/n, 1$ and its maximum value of

$$h_{\mathrm{m}} = h\left(\frac{a}{n}\right) = 2 \left[\frac{3\bar{Q}m}{5n\pi \sin\alpha} \right]^{1/3} \tag{15}$$

$n/2$ times in $0 \le y \le a$ at $y/a = 1/n, 3/n, \ldots, (n-1)/n$. In particular,

$$a \sim n\pi \left(\alpha - \frac{\pi}{2}\right)^{-1/2} \to \infty, \quad h_{\mathrm{m}} \sim 2 \left[\frac{3\bar{Q}}{5n\pi}\right]^{1/3} \left(\alpha - \frac{\pi}{2}\right)^{1/6} \to 0 \tag{16}$$

as $\alpha \to \pi/2^+$, and

$$a = n\pi + \frac{n\pi}{4}(\pi - \alpha)^2 + O(\pi - \alpha)^4, \quad h_{\mathrm{m}} \sim 2 \left[\frac{3\bar{Q}}{5n\pi(\pi - \alpha)}\right]^{1/3} \to \infty \tag{17}$$

as $\alpha \to \pi^-$. Note that all of these solutions are physically realisable and that the higher-branch solutions (i.e. those for $n = 2, 3, \ldots$) are simply "arrays" of n identical contiguous rivulets each of which is a (suitably rescaled) copy of the lowest-branch ($n = 1$) solution. Presumably these higher-branch solutions would be rather difficult to achieve in practice! Physically these solutions correspond to rivulets running continuously from $\alpha = \pi/2$ (where

8

they become infinitely wide and vanishingly thin according to (16) as $\alpha \to \pi/2^+$) to $\alpha = \pi$ (where they become infinitely deep with finite semi-width $n\pi$ according to (17) as $\alpha \to \pi^-$). Note that this behaviour is qualitatively different from the corresponding behaviour in the non-perfectly wetting case discussed by Duffy & Moffatt (1995) and Wilson & Duffy (1998, Section V). In particular, in the non-perfectly wetting case there is a physically realisable solution for *all* values of α representing a rivulet running continuously from $\alpha = 0$ to $\alpha = \pi$, and the higher-branch solutions are not physically realisable.

Figure 2 shows a and $h_{\mathrm{m}}/\bar{Q}^{1/3}$ plotted as functions of α/π for a range of values of n. Figure 3 shows typical scaled lowest-branch ($n = 1$) transverse rivulet profiles $h/\bar{Q}^{1/3}$ plotted as functions of y for a range of values of α.

4 The General Case $H \not\equiv 0$

In the general case $H \not\equiv 0$ the substrate is *not* locally planar. Solving (8) subject to (6) at $y = \pm a$ yields

$$h(y) = -aH'(a)f(M,Y) + H(a) - H(y), \qquad (18)$$

where the function $f = f(M,Y)$ is defined by

$$f(M,Y) = \begin{cases} \dfrac{\cosh M - \cosh MY}{M \sinh M} & \text{if} \quad 0 \le \alpha < \pi/2, \\[2mm] \dfrac{1 - Y^2}{2} & \text{if} \quad \alpha = \pi/2, \\[2mm] \dfrac{\cos MY - \cos M}{M \sin M} & \text{if} \quad \pi/2 < \alpha \le \pi, \end{cases} \qquad (19)$$

and we have introduced the notation $M = ma$ and $Y = y/a$. Note that the solution in the planar case discussed in section 3 is *not* recovered simply by setting $H \equiv 0$ in (18). Note also that the function $f(M,Y)$ defined in (19) differs from the corresponding function $f(y)$ used by Wilson & Duffy (1998, Equation 16) by a factor of a.

For any prescribed positive value of the flux, $\bar{Q} > 0$, the possible rivulet semi-widths are the positive solutions for a of the equation $Q = \bar{Q}$, where Q is given by (11) with h given by

9

(18). Once a is known h is given explicitly by (18).

Thus far the analysis is valid for a general symmetric transverse substrate profile $H(y)$. Henceforth for simplicity we shall follow Wilson & Duffy (1998) and restrict our attention to a general symmetric power-law profile in the form

$$H(y) = A|y|^p, \tag{20}$$

where both the non-zero coefficient $A \neq 0$ and the positive exponent $p > 0$ are constants. Positive or negative values of A correspond to locally concave or convex substrates respectively. The special case $p = 2$ corresponds to a locally parabolic substrate with constant curvature $2A$. With the choice (20) for H the solution for h given by (18) can be written as

$$h = Aa^p \left[-pf(M,Y) + 1 - |Y|^p \right] \tag{21}$$

and so from (11) the flux Q can be written as

$$Q = \frac{2 \sin \alpha A^3}{3m^{3p+1}} F(M,p), \tag{22}$$

where the function $F(M,p)$ is defined by

$$F(M,p) = M^{3p+1} \int_0^1 \left[-p\,f(M,Y) + 1 - Y^p \right]^3 \, \mathrm{d}Y. \tag{23}$$

In particular, equations (21) and (22) imply that a and $h/\bar{Q}^{1/3}$ depend on the parameters $\bar{Q}$ and A only in the combination $A^3/\bar{Q}$. Evidently determining the behaviour of F and hence Q is key to understanding the behaviour of the possible rivulet solutions. The asymptotic behaviours of the function f and hence of the function F in the limits $M \to 0$, $M \to \infty$ and $M \to n\pi$ ($n = 1, 2, 3, \ldots$) are given in Appendix A for future reference.

For any given value of the exponent $p > 0$ the function F and hence the flux Q can, in principle, be determined explicitly. Since the algebra required to calculate F is, in general, rather lengthy we used the symbolic algebra packages MAPLE and MATHEMATICA to perform the analytical evaluation of Q as well as the subsequent numerical calculation of a from

10

the algebraic equation $Q = \bar{Q}$. The efficient numerical procedure used to obtain the plots of a as a function of α given in the present paper is described in Appendix B.

The critical condition $h(0) = 0$ for the solution (21) to be physically realisable gives $pf(M,0) = 1$, i.e. $M\coth(M/2) = p$ in $0 \leq \alpha < \pi/2$ and $M\cot(M/2) = p$ in $\pi/2 < \alpha \leq \pi$. The solutions of these two equations are denoted by $M = M^*$ and the corresponding values of F by $F^* = F(M^*, p)$. On the other hand, the critical condition $h''(a) = 0$ gives the equations $1 + M\coth M = p$ in $0 \leq \alpha < \pi/2$ and $1 + M\cot M = p$ in $\pi/2 < \alpha \leq \pi$.

As in the non-perfectly wetting case studied by Wilson & Duffy (1998) and in the locally planar case discussed in section 3 there are, in general, infinitely many branches of solutions for a in $\pi/2 < \alpha \leq \pi$; however for simplicity we shall hereafter restrict our attention to the lowest branch of solutions satisfying $0 \leq a \leq \pi/m$ (i.e. $0 \leq M \leq \pi$) in $\pi/2 < \alpha \leq \pi$ unless it is stated otherwise.

Figure 4 shows plots of $F(M,p)$ as a function of M in the cases $\cos\alpha > 0$, $\cos\alpha = 0$ and $\cos\alpha < 0$ for $p = 1$, $p = 2$ and $p = 3$. When $\cos\alpha \geq 0$ all values of $M \geq 0$ are relevant, but when $\cos\alpha < 0$ we restrict our attention to values of M satisfying $0 \leq M \leq \pi$. As Fig. 4 shows, the form of F is qualitatively different for $p < 2$, $p = 2$ and $p > 2$. The form of F when $p = 1$ shown in Fig. 4(a) is typical of that for all values of p satisfying $p < 2$, and the form of F when $p = 3$ shown in Fig. 4(c) is typical of that for all values of p satisfying $p > 2$. As Fig. 4(a) illustrates, when $p < 2$ then F increases monotonically from zero to $+\infty$ with M when $\cos\alpha \geq 0$. However, when $\cos\alpha < 0$ then F initially increases from zero with M before reaching a maximum value $F_{\max} = F(M_{\max}, p) > 0$ at $M = M_{\max}$ and then decreases monotonically as M increases; specifically $F = 0$ at some value $M = M_0$ ($> M_{\max}$), and $F \to -\infty$ according to (A.8) with $n = 1$ as $M \to \pi^-$. As Fig. 4(b) illustrates, in the special case $p = 2$ then F increases monotonically from zero to $+\infty$ with M when $\cos\alpha > 0$, is identically equal to zero when $\cos\alpha = 0$, and decreases monotonically from zero to $-\infty$ with

M when $\cos\alpha < 0$. As Fig. 4(c) illustrates, when $p > 2$ then F decreases monotonically from zero to $-\infty$ with M when $\cos\alpha \le 0$. However, when $\cos\alpha > 0$ then F initially decreases from zero with M before reaching a minimum value $F_{\min} = F(M_{\min}, p) < 0$ at $M = M_{\min}$ and then increases monotonically as M increases; specifically $F = 0$ at some value $M = M_0$ ($> M_{\min}$), and $F \to \infty$ according to (A.6) as $M \to \infty$.

Differentiation of (23) shows that $M_{\max}$ and $M_{\min}$ satisfy $1 + M\cot M = p$ and $1 + M\coth M = p$, respectively. These equations are exactly the same as those obtained earlier for the critical condition $h''(a) = 0$, showing that the non-zero stationary points of F correspond to the critical physically realisable solution satisfying $h''(a) = 0$.

Numerically calculated values of $M_{\max}$, $M_{\min}$, M_0 and M^* together with $F_{\max}$, $F_{\min}$ and F^* are plotted as functions of p in Fig. 5. Note that $F_{\max}$ and $M_{\max}$ are defined only for $p < 2$, while $F_{\min}$ and $M_{\min}$ are defined only for $p > 2$. As Fig. 5(a) shows, $M_{\max}$, M_0 and M^* decrease monotonically with p in $0 < p < 2$ (from approximately 2.028758, 2.891093 and π respectively as $p \to 0^+$, to zero as $p \to 2$), and that $M_{\min}$, M_0 and M^* increase monotonically from zero with p in $p > 2$. Moreover careful asymptotic analysis reveals that $M_{\max} \sim (3(2-p))^{1/2} \to 0$ as $p \to 2^-$, $M_{\min} \sim (3(p-2))^{1/2} \to 0$ as $p \to 2^+$, $M_0 \sim |k_1(2-p)|^{1/2} \to 0$ (with $k_1 \simeq 5.216666$) and $M^* \sim |6(2-p)|^{1/2} \to 0$ as $p \to 2$, $M_{\min} \sim p - 1 \to \infty$, $M_0 \sim p \to \infty$ and $M^* \sim p \to \infty$ as $p \to \infty$, and hence $F_{\max} \sim k_2 p^3 \to 0^+$ (with $k_2 \simeq 5.565160$) and $F^* \to -5\pi/16$ as $p \to 0^+$, $F_{\max} \sim k_3(2-p)^{13/2} \to 0^+$ (with $k_3 \simeq 0.138892$) and $F^* \sim -k_4(2-p)^{13/2} \to 0^-$ (with $k_4 \simeq 0.099352$) as $p \to 2^-$, $F_{\min} \sim -k_3(p-2)^{13/2} \to 0^-$ and $F^* \sim k_4(p-2)^{13/2} \to 0^+$ as $p \to 2^+$, and $F_{\min} \sim -p^{3p}/3 \to -\infty$ and $F^* \sim 10p^{3(p-1)}/243 \to \infty$ as $p \to \infty$.

Using the information about the behaviour of the function F (and hence Q) described above we can now determine the qualitatively different behaviour of the rivulet solutions in the cases $p < 2$, $p = 2$ and $p > 2$. In all three cases the solutions for locally concave ($A > 0$) and locally convex ($A < 0$) substrates are also qualitatively different.

4.1 The Limit $\alpha \to 0^+$

In the limit $\alpha \to 0^+$ (i.e. near the top of the cylinder) from (22) we must have $F \to \infty$ according to (A.6) and hence

$$a \sim \left[\frac{(p+1)(2p+1)(3p+1)\bar{Q}}{4p^3 \alpha A^3} \right]^{1/(3p+1)} \to \infty \tag{24}$$

as $\alpha \to 0^+$. Using (A.5) in (21) we obtain

$$h \sim A \left[\frac{(p+1)(2p+1)(3p+1)\bar{Q}}{4p^3 \alpha A^3} \right]^{p/(3p+1)} \left(1 - \frac{|y|^p}{a^p} \right) \to \infty \tag{25}$$

as $\alpha \to 0^+$. In particular, (24) and (25) show that the rivulet becomes infinitely wide and deep as $\alpha \to 0^+$ when the substrate is locally concave (i.e. when $A > 0$), but that there is *no* solution near $\alpha = 0$ when the substrate is locally convex (i.e. when $A < 0$). Note that in this limit $H + h \sim H(a)$ and the free surface of the rivulet becomes flat away from the contact lines. This behaviour is illustrated by Fig. 6 which shows typical scaled transverse rivulet profiles $(H + h)/\bar{Q}^{1/3}$ plotted as functions of y for a range of values of α near $\alpha = 0$ in the case $p = 2$ and $A^3/\bar{Q} = 1$. Note also that (24) coincides with the corresponding result in the non-perfectly wetting case obtained by Wilson & Duffy (1998, Equation 34), showing that contact-angle effects play only a minor role in this limit.

4.2 The Limit $\alpha \to \pi/2$

In the limit $\alpha \to \pi/2$ (i.e. when the substrate is nearly vertical) from (22) we must have $F \to 0$ and hence either $ma \to 0$ (which occurs for all values of p *including* $p = 2$) or $ma \to M_0$ (which occurs for all values of p *except* $p = 2$), corresponding to three rather different types of rivulet behaviour.

(a) The Case $ma \to 0$

In the case $ma \to 0$ the behaviour depends on whether $p = 2$ or $p \neq 2$ (i.e. on whether or not the substrate is locally parabolic).

13

In the general case $p \neq 2$ in which the substrate is not locally parabolic we have

$$a = a_0 + a_1 \left(\alpha - \frac{\pi}{2} \right) + O \left(\alpha - \frac{\pi}{2} \right)^2 \tag{26}$$

as $\alpha \to \pi/2$, and using (A.1) in (21) we obtain

$$h = h_0 + h_1 \left(\alpha - \frac{\pi}{2} \right) + O \left(\alpha - \frac{\pi}{2} \right)^2, \tag{27}$$

where the functions $h_0 = h_0(y)$ and $h_1 = h_1(y)$ are given by

$$h_0 = A a_0^p \left[-p \frac{a_0^2 - y^2}{2a_0^2} + 1 - \frac{|y|^p}{a_0^p} \right], \tag{28}$$

$$h_1 = -\frac{pA a_0^{p-3}}{24} (a_0^2 - y^2) \left[a_0(a_0^2 - y^2) + 12a_1(p - 2) \right], \tag{29}$$

and using (A.2) in (22) yields

$$Q = \frac{2A^3 a_0^{3p+1}}{3} \left[F_0 + \frac{(3p + 1)a_1 F_0 - a_0^3 F_1}{a_0} \left(\alpha - \frac{\pi}{2} \right) + O \left(\alpha - \frac{\pi}{2} \right)^2 \right], \tag{30}$$

where F_0 and F_1 are given by (A.3) and (A.4) respectively. Hence we deduce that

$$a_0 = \left(\frac{3\bar{Q}}{2F_0 A^3} \right)^{1/(3p+1)} \tag{31}$$

and

$$a_1 = \frac{F_1 a_0^3}{(3p + 1)F_0}. \tag{32}$$

In particular, since F_0 has the same sign as $2 - p$, equation (31) shows that when the substrate is locally concave (i.e. when $A > 0$) a solution of this kind is possible only when $p < 2$, and when the substrate is locally convex (i.e. when $A < 0$) a solution is possible only when $p > 2$. In addition, since $F_1 > 0$, equation (32) shows that $a_1 = da/d\alpha$ evaluated at $\alpha = \pi/2$ is *positive* when $p < 2$ and *negative* when $p > 2$. The solutions for h_0, a_0 and a_1/a_0^3 in the cases $p = 1, 3, 4, 5$ and 6 are listed in Table 1 for reference. Note that there is no solution of this kind in the special case $p = 2$.

14

In the special case $p = 2$ in which the substrate is locally parabolic, using (A.2) in (22) yields

$$a \sim \left[\frac{243243\bar{Q}}{32A^3} \right]^{1/13} \left(\frac{\pi}{2} - \alpha \right)^{-3/13} \to \infty \tag{33}$$

as $\alpha \to \pi/2$, and using (A.1) in (21) we obtain

$$h \sim \frac{A}{12} \left[\frac{243243\bar{Q}}{32A^3} \right]^{4/13} \left(1 - \frac{y^2}{a^2} \right)^2 \left(\frac{\pi}{2} - \alpha \right)^{1/13} \to 0 \tag{34}$$

as $\alpha \to \pi/2$. In particular, (33) and (34) show that when $p = 2$ the rivulet becomes infinitely wide and vanishingly thin as $\alpha \to \pi/2$. Furthermore a solution of this kind on a locally concave parabolic substrate (i.e. when $p = 2$ and $A > 0$) is possible only as $\alpha \to \pi/2^-$ and a solution on a locally convex parabolic substrate (i.e. when $p = 2$ and $A < 0$) is possible only as $\alpha \to \pi/2^+$.

(b) The Case $ma \to M_0$

In the case $ma \to M_0$ if $F = 0$ in $\cos \alpha > 0$ (as it does when $p > 2$) then

$$a \sim M_0 \left(\frac{\pi}{2} - \alpha \right)^{-1/2} \to \infty \tag{35}$$

as $\alpha \to \pi/2^-$, while if $F = 0$ in $\cos \alpha < 0$ (as it does when $p < 2$) then

$$a \sim M_0 \left(\alpha - \frac{\pi}{2} \right)^{-1/2} \to \infty \tag{36}$$

as $\alpha \to \pi/2^+$. In both cases from (21) we obtain

$$h \sim Aa^p \left[-pf \left(M_0, \frac{y}{a} \right) + 1 - \frac{|y|^p}{a^p} \right] \to \infty. \tag{37}$$

In particular, (35)–(37) show that the rivulet becomes infinitely wide and deep as $\alpha \to \pi/2^-$ for $p > 2$ and as $\alpha \to \pi/2^+$ for $p < 2$. Note that there is no solution of this kind in the special case $p = 2$.

15

4.3 Limit $\alpha \to \pi^-$

In the limit $\alpha \to \pi^-$ (i.e. near the bottom of the cylinder) from (22) we must have $|F| \to \infty$ according to (A.8) and hence

$$a \sim n\pi + pA(n\pi)^{p-1} \left[\frac{5n\pi(\pi - \alpha)}{3\bar{Q}} \right]^{1/3} \tag{38}$$

as $\alpha \to \pi^-$. Using (A.7) in (21) we obtain

$$h \sim \left[\frac{3\bar{Q}}{5n\pi(\pi - \alpha)} \right]^{1/3} [1 - (-1)^n \cos y] \to \infty \tag{39}$$

as $\alpha \to \pi^-$. Thus in this limit a approaches $n\pi$ from *above* when the substrate is locally concave (i.e. when $A > 0$) and from *below* when it is locally convex (i.e. when $A < 0$). In particular, if we restrict our attention to lowest-branch solutions satisfying $0 \leq a \leq \pi/m$ in $\pi/2 < \alpha \leq \pi$, then (38) and (39) with $n = 1$ show that the rivulet becomes infinitely deep with finite semi-width π as $\alpha \to \pi^-$ when the substrate is locally convex (i.e. when $A < 0$), but that there is *no* solution near $\alpha = \pi$ when the substrate is locally concave (i.e. when $A > 0$).

5 Solution for $p < 2$

When the substrate is locally concave (i.e. when $A > 0$) there is one solution for a in $0 \leq \alpha \leq \pi/2$, two solutions in $\pi/2 < \alpha < \alpha_{max}$, and one solution at $\alpha = \alpha_{max}$, where $\alpha_{max} = \alpha_{max}(A^3/\bar{Q}, p)$ ($\pi/2 < \alpha_{max} < \pi$) denotes the critical value of α corresponding to $M = M_{max}$ and so satisfies

$$\frac{2A^3 F_{max}}{3\bar{Q}} \sin \alpha_{max} = |\cos \alpha_{max}|^{(3p+1)/2}. \tag{40}$$

Physically these solutions correspond to a rivulet running continuously from $\alpha = 0$ (where it becomes infinitely wide and deep according to (24) and (25) as $\alpha \to 0^+$) through $\alpha = \pi/2$ (where $a = a_0$, $h = h_0$ and $da/d\alpha > 0$) to $\alpha = \alpha_{max}$ (where $a = a_{max} = M_{max}|\cos \alpha_{max}|^{-1/2}$). Note that the second solution for a in $\pi/2 < \alpha < \alpha_{max}$, which satisfies $a \to \infty$ according to (36)

16

as $\alpha \to \pi/2^+$ and connects with the first solution at $\alpha = \alpha_{\mathrm{max}}$, is *never* physically realisable since it always satisfies $h''(a) < 0$.

On the other hand, when the substrate is locally convex (i.e. when $A < 0$) there is no solution for a in $0 \le \alpha \le \pi/2$ and one solution in $\pi/2 < \alpha \le \pi$. This solution satisfies $a \to \infty$ according to (36) as $\alpha \to \pi/2^+$, and $a \to \pi^-$ according to (38) with $n = 1$ as $\alpha \to \pi^-$. This solution is physically realisable in $\alpha^* \le \alpha \le \pi$ but *not* in $\pi/2 < \alpha < \alpha^*$ in which interval it satisfies $h(0) < 0$, where $\alpha^* = \alpha^*(A^3/\bar{Q}, p)$ ($\pi/2 < \alpha^* < \pi$) denotes the critical value of α corresponding to $M = M^*$ and so satisfies

$$\frac{2A^3 F^*}{3\bar{Q}} \sin \alpha^* = |\cos \alpha^*|^{(3p+1)/2}. \tag{41}$$

Physically this solution corresponds to a rivulet running continuously from $\alpha = \alpha^*$ (where $a = a^* = M^*|\cos \alpha^*|^{-1/2}$) to $\alpha = \pi$ (where it becomes infinitely deep with semi-width π according to (38) and (39) with $n = 1$ as $\alpha \to \pi^-$).

Figure 7(a) shows a sketch of a plotted as a function of α when $p < 2$ for both $A > 0$ and $A < 0$ which illustrates all of the features described above. In particular, Fig. 7(a) shows how the solutions for $A > 0$ fail to be physically realisable via $h''(a) = 0$ at $\alpha = \alpha_{\mathrm{max}}$, and solutions for $A < 0$ fail to be physically realisable via $h(0) = 0$ at $\alpha = \alpha^*$. Figure 7(a) also shows how the curve $a = M_0 |\cos \alpha|^{-1/2}$ in $\pi/2 < \alpha \le \pi$ separates the (α, a) plane into regions containing the solutions for $A > 0$ and $A < 0$.

Figure 7(b) shows numerically calculated values of a plotted as a function of α/π for a range of both positive and negative values of $A/\bar{Q}^{1/3}$ in the case $p = 1$. In this case $M_{\mathrm{max}} = \pi/2$, $F_{\mathrm{max}} = (3\pi^4 + 36\pi^2 - 576\pi + 1168)/192 \simeq 0.031123$, $M_0 \simeq 2.151041$, $M^* \simeq 2.331122$ and $F^* \simeq -0.047340$. Note that in this case α_{max} and α^* are given explicitly by

$$\alpha_{\mathrm{max}} = \pi - \sin^{-1}\left(-\frac{A^3 F_{\mathrm{max}}}{3\bar{Q}} + \left[\frac{A^6 F_{\mathrm{max}}^2}{9\bar{Q}^2} + 1\right]^{1/2}\right) \tag{42}$$

17

and

$$\alpha^* = \pi - \sin^{-1}\left(-\frac{A^3 F^*}{3\bar{Q}} + \left[\frac{A^6 F^{*2}}{9\bar{Q}^2} + 1\right]^{1/2}\right). \tag{43}$$

Figure 8 shows numerically calculated values of α_{max} and α^* together with a_{max} and a^* plotted as functions of $A/\bar{Q}^{1/3}$ in the case $p = 1$. Note that α_{max} and a_{max} are defined only for $A > 0$, while α^* and a^* are defined only for $A < 0$. As Fig. 8 shows, in this case α_{max} is a monotonically increasing function of $A/\bar{Q}^{1/3}$ satisfying $\alpha_{\mathrm{max}} \to \pi/2^+$ as $A/\bar{Q}^{1/3} \to 0^+$ and $\alpha_{\mathrm{max}} \to \pi^-$ as $A/\bar{Q}^{1/3} \to \infty$, α^* is a monotonically decreasing function of $A/\bar{Q}^{1/3}$ satisfying $\alpha^* \to \pi^-$ as $A/\bar{Q}^{1/3} \to -\infty$ and $\alpha^* \to \pi/2^+$ as $A/\bar{Q}^{1/3} \to 0^-$, a_{max} is a monotonically decreasing function of $A/\bar{Q}^{1/3}$ satisfying $a_{\mathrm{max}} \to \infty$ as $A/\bar{Q}^{1/3} \to 0^+$ and $a_{\mathrm{max}} \to M_{\mathrm{max}}^+$ as $A/\bar{Q}^{1/3} \to \infty$, and a^* is a monotonically increasing function of $A/\bar{Q}^{1/3}$ satisfying $a^* \to M^{*+}$ as $A/\bar{Q}^{1/3} \to -\infty$ and $a^* \to \infty$ as $A/\bar{Q}^{1/3} \to 0^-$. Setting $p = 1$ in (24) and (25) shows that if $A > 0$ then

$$a \sim \left(\frac{6\bar{Q}}{\alpha A^3}\right)^{1/4} \to \infty, \quad h \sim A\left(\frac{6\bar{Q}}{\alpha A^3}\right)^{1/4}\left(1 - \frac{|y|}{a}\right) \to \infty \tag{44}$$

as $\alpha \to 0^+$, setting $p = 1$ in (31) and (28) shows that if $A > 0$ then

$$a = a_0 = \left(\frac{84\bar{Q}}{A^3}\right)^{1/4}, \quad h = h_0 = \frac{A}{2a_0}\left(a_0 - |y|\right)^2 \tag{45}$$

at $\alpha = \pi/2$, while setting $p = 1$ and $n = 1$ in (38) and (39) shows that if $A < 0$ then

$$a \sim \pi + A\left[\frac{5\pi(\pi - \alpha)}{3\bar{Q}}\right]^{1/3}, \quad h \sim \left[\frac{3\bar{Q}}{5\pi(\pi - \alpha)}\right]^{1/3}(1 + \cos y) \to \infty \tag{46}$$

as $\alpha \to \pi^-$. Figure 9 shows typical scaled transverse rivulet profiles $(H + h)/\bar{Q}^{1/3}$ plotted as functions of y for a range of values of α for $A/\bar{Q}^{1/3} = 1$ and $A/\bar{Q}^{1/3} = -1$.

6 Solution in the Special Case $p = 2$

When the substrate is locally concave (i.e. when $A > 0$) there is one solution for a in $0 \leq \alpha < \pi/2$ and no solution in $\pi/2 \leq \alpha \leq \pi$. This solution is *always* physically realisable and

18

corresponds to a rivulet running continuously from $\alpha = 0$, where it becomes infinitely wide and deep according to (24) and (25) with $p = 2$, i.e.

$$a \sim \left(\frac{105\bar{Q}}{32\alpha A^3} \right)^{1/7} \to \infty, \quad h \sim A \left(\frac{105\bar{Q}}{32\alpha A^3} \right)^{2/7} \left(1 - \frac{y^2}{a^2} \right) \to \infty \qquad (47)$$

as $\alpha \to 0^+$, to $\alpha = \pi/2$, where it becomes infinitely wide and vanishingly thin according to (33) and (34) as $\alpha \to \pi/2^-$.

On the other hand, when the substrate is locally convex (i.e. when $A < 0$) there is no solution for a in $0 \leq \alpha \leq \pi/2$ and one solution in $\pi/2 < \alpha \leq \pi$. This solution is again *always* physically realisable and corresponds to a rivulet running continuously from $\alpha = \pi/2$, where it becomes infinitely wide and vanishingly thin according to (33) and (34) as $\alpha \to \pi/2^+$, to $\alpha = \pi$, where it becomes infinitely deep with semi-width π according to (38) and (39) with $p = 2$ and $n = 1$, i.e.

$$a \sim \pi + 2A\pi \left[\frac{5\pi(\pi - \alpha)}{3\bar{Q}} \right]^{1/3}, \quad h \sim \left[\frac{3\bar{Q}}{5\pi(\pi - \alpha)} \right]^{1/3} (1 + \cos y) \to \infty \qquad (48)$$

as $\alpha \to \pi^-$.

Figure 10(a) shows a sketch of a plotted as a function of α in the special case $p = 2$ for both $A > 0$ and $A < 0$ which illustrates all of the features described above.

Figure 10(b) shows numerically calculated values of a plotted as a function of α/π for a range of both positive and negative values of $A/\bar{Q}^{1/3}$ in the special case $p = 2$. Figure 11 shows typical scaled transverse rivulet profiles $(H + h)/\bar{Q}^{1/3}$ plotted as functions of y for a range of values of α for $A/\bar{Q}^{1/3} = 1$ and $A/\bar{Q}^{1/3} = -1$.

7   Solution for $p > 2$

When the substrate is locally concave (i.e. when $A > 0$) there is one solution for a in $0 \leq \alpha < \pi/2$ and no solution in $\pi/2 \leq \alpha \leq \pi$. This solution satisfies $a \to \infty$ according to (24) as $\alpha \to 0^+$, and $a \to \infty$ according to (35) as $\alpha \to \pi/2^-$. This solution is physically

19

realisable in $0 \leq \alpha \leq \alpha^*$ but *not* in $\alpha^* < \alpha < \pi/2$ in which interval it satisfies $h(0) < 0$, where $\alpha^* = \alpha^*(A^3/\bar{Q}, p)$ $(0 < \alpha^* < \pi/2)$ again denotes the critical value of α corresponding to $M = M^*$ and so again satisfies (41). Physically this solution corresponds to a rivulet running continuously from $\alpha = 0$ (where it becomes infinitely wide and deep according to (24) and (25) as $\alpha \to 0^+$) to $\alpha = \alpha^*$ (where $a = a^* = M^*(\cos \alpha^*)^{-1/2}$).

On the other hand, when the substrate is locally convex (i.e. when $A < 0$) there is one solution for a at $\alpha = \alpha_{\min}$, two solutions in $\alpha_{\min} < \alpha < \pi/2$ and one solution in $\pi/2 \leq \alpha \leq \pi$, where $\alpha_{\min} = \alpha_{\min}(A^3/\bar{Q}, p)$ $(0 < \alpha_{\min} < \pi/2)$ denotes the critical value of α corresponding to $M = M_{\min}$ and so satisfies

$$\frac{2A^3 F_{\min}}{3\bar{Q}} \sin \alpha_{\min} = (\cos \alpha_{\min})^{(3p+1)/2}. \tag{49}$$

Physically these solutions correspond to a rivulet running continuously from $\alpha = \alpha_{\min}$ (where $a = a_{\min} = M_{\min}(\cos \alpha_{\min})^{-1/2}$) through $\alpha = \pi/2$ (where $a = a_0$, $h = h_0$ and $da/d\alpha < 0$) to $\alpha = \pi$ (where it becomes infinitely deep with semi-width π according to (38) and (39) with $n = 1$ as $\alpha \to \pi^-$). Note that the second solution for a in $\alpha_{\min} < \alpha < \pi/2$, which connects with the first solution at $\alpha = \alpha_{\min}$ and satisfies $a \to \infty$ according to (35) as $\alpha \to \pi/2^-$, is *never* physically realisable since it always satisfies $h''(a) < 0$.

Figure 12(a) shows a sketch of a plotted as a function of α when $p > 2$ for both $A > 0$ and $A < 0$ which illustrates all of the features described above. In particular, Fig. 12(a) shows how the solutions for $A > 0$ fail to be physically realisable via $h(0) = 0$ at $\alpha = \alpha^*$ and solutions for $A < 0$ fail to be physically realisable via $h''(a) = 0$ at $\alpha = \alpha_{\min}$. Figure 12(a) also shows how the curve $a = M_0(\cos \alpha)^{-1/2}$ in $0 \leq \alpha < \pi/2$ separates the (α, a) plane into regions containing the solutions for $A > 0$ and $A < 0$.

Figure 12(b) shows numerically calculated values of a plotted as a function of α/π for a range of both positive and negative values of $A/\bar{Q}^{1/3}$ in the case $p = 3$. In this case $M_{\min} \simeq 1.915008$, $F_{\min} \simeq -0.715583$, $M_0 \simeq 2.430916$, $M^* \simeq 2.575679$ and $F^* \simeq 0.393046$. Figure 8 shows

20

numerically calculated values of $\alpha_{\min}$ and α^* together with $a_{\min}$ and a^* plotted as functions of $A/\bar{Q}^{1/3}$ in the case $p = 3$. Note that $\alpha_{\min}$ and $a_{\min}$ are defined only for $A < 0$, while α^* and a^* are defined only for $A > 0$. As Fig. 8 shows, in this case $\alpha_{\min}$ is a monotonically increasing function of $A/\bar{Q}^{1/3}$ satisfying $\alpha_{\min} \to 0^+$ as $A/\bar{Q}^{1/3} \to -\infty$ and $\alpha_{\min} \to \pi/2^-$ as $A/\bar{Q}^{1/3} \to 0^-$, α^* is a monotonically decreasing function of $A/\bar{Q}^{1/3}$ satisfying $\alpha^* \to \pi/2^-$ as $A/\bar{Q}^{1/3} \to 0^+$ and $\alpha^* \to 0^+$ as $A/\bar{Q}^{1/3} \to \infty$, $a_{\min}$ is a monotonically increasing function of $A/\bar{Q}^{1/3}$ satisfying $a_{\min} \to M_{\min}^+$ as $A/\bar{Q}^{1/3} \to -\infty$ and $a_{\min} \to \infty$ as $A/\bar{Q}^{1/3} \to 0^-$, and a^* is a monotonically decreasing function of $A/\bar{Q}^{1/3}$ satisfying $a^* \to \infty$ as $A/\bar{Q}^{1/3} \to 0^+$ and $a^* \to M^{*+}$ as $A/\bar{Q}^{1/3} \to \infty$. Setting $p = 3$ in (24) and (25) shows that if $A > 0$ then

$$a \sim \left(\frac{70\bar{Q}}{27\alpha A^3}\right)^{1/10} \to \infty, \quad h \sim A \left(\frac{70\bar{Q}}{27\alpha A^3}\right)^{3/10} \left(1 - \frac{|y|^3}{a^3}\right) \to \infty \qquad (50)$$

as $\alpha \to 0^+$, setting $p = 3$ in (31) and (28) shows that if $A < 0$ then

$$a = a_0 = \left(-\frac{1680\bar{Q}}{43A^3}\right)^{1/10}, \quad h = h_0 = -\frac{A}{2}\left(a_0 + 2|y|\right)\left(a_0 - |y|\right)^2 \qquad (51)$$

at $\alpha = \pi/2$, while setting $p = 3$ and $n = 1$ in (38) and (39) shows that if $A < 0$ then

$$a \sim \pi + 3A\pi^2 \left[\frac{5\pi(\pi - \alpha)}{3\bar{Q}}\right]^{1/3}, \quad h \sim \left[\frac{3\bar{Q}}{5\pi(\pi - \alpha)}\right]^{1/3} (1 + \cos y) \to \infty \qquad (52)$$

as $\alpha \to \pi^-$. Figure 13 shows typical scaled transverse rivulet profiles $(H + h)/\bar{Q}^{1/3}$ plotted as functions of y for a range of values of α for $A/\bar{Q}^{1/3} = 1$ and $A/\bar{Q}^{1/3} = -1$.

8 The Limit $A^3/\bar{Q} \to 0$

In the limit $A^3/\bar{Q} \to 0$, corresponding to a weakly non-planar substrate and/or a large volume flux, the asymptotic behaviour of the solution is qualitatively different in $0 \le \alpha < \pi/2$, $\alpha = \pi/2$ and $\pi/2 < \alpha \le \pi$.

In $0 \le \alpha < \pi/2$ there is no solution as $A^3/\bar{Q} \to 0^-$, but from (21), (22), (A.5) and (A.6) we have

$$a \sim \left[\frac{(p+1)(2p+1)(3p+1)\bar{Q}}{4p^3 \sin \alpha A^3}\right]^{1/(3p+1)} \to \infty \qquad (53)$$

and

$$h \sim A \left[\frac{(p+1)(2p+1)(3p+1)\bar{Q}}{4p^3 \sin \alpha A^3} \right]^{p/(3p+1)} \left(1 - \frac{|y|^p}{a^p} \right) \tag{54}$$

as $A^3/\bar{Q} \to 0^+$. Note that in this case $H + h \sim H(a)$ and that the free surface of the rivulet becomes flat away from the contact lines in this limit. When $\alpha = \pi/2$ we have $a = a_0 \to \infty$ and $h = h_0$, where a_0 and h_0 are given by (31) and (28) respectively, and so there is a solution as $A^3/\bar{Q} \to 0^+$ when $p < 2$, and as $A^3/\bar{Q} \to 0^-$ when $p > 2$, but not otherwise. Thus in $0 \le \alpha \le \pi/2$ the rivulet becomes infinitely wide and vanishingly thin in the limit of a weakly non-planar substrate $A \to 0$, but infinitely wide and deep in the limit of a large volume flux $\bar{Q} \to \infty$. In $\pi/2 < \alpha \le \pi$ from (21), (22), (A.7) and (A.8) we have

$$a \sim \frac{n\pi}{m} + \frac{pA}{m^2} \left(\frac{n\pi}{m} \right)^{p-1} \left[\frac{5n\pi \sin \alpha}{3\bar{Q}m} \right]^{1/3} \tag{55}$$

and

$$h \sim \left[\frac{3\bar{Q}m}{5n\pi \sin \alpha} \right]^{1/3} \left[1 - (-1)^n \cos my \right] \tag{56}$$

as $A^3/\bar{Q} \to 0$, and so there is a lowest-branch ($n = 1$) solution satisfying $0 \le a \le \pi/m$ in $\pi/2 < \alpha \le \pi$ as $A^3/\bar{Q} \to 0^-$, but not as $A^3/\bar{Q} \to 0^+$. Thus in $\pi/2 < \alpha \le \pi$ the rivulet has finite width and thickness in the limit of a weakly non-planar substrate $A \to 0$, but becomes infinitely deep with finite width in the limit of large volume flux $\bar{Q} \to \infty$. In particular, (55) and (56) show that, as expected, the solution for a locally planar substrate ($H \equiv 0$) described in section 3 is recovered at leading order in the limit $A \to 0$.

9 The Limit $A^3/\bar{Q} \to \infty$

In the limit $A^3/\bar{Q} \to \infty$, corresponding to a strongly concave substrate and/or a small volume flux down a concave substrate, the asymptotic behaviour is qualitatively different for $p \ne 2$ and $p = 2$.

In the general case $p \neq 2$ there are two rather different kinds of behaviour in this limit. Firstly, from (21) and (22) we have

$$a \sim \frac{M_0}{m} \qquad (57)$$

and h is given by (37) as $A^3/\bar{Q} \to \infty$ in $\pi/2 < \alpha < \pi$ when $p < 2$ and in $0 < \alpha < \pi/2$ when $p > 2$, but not otherwise; however, this solution is never physically realisable. Secondly, from (21)–(23), (A.1) and (A.2) we have

$$a \sim \left(\frac{3\bar{Q}}{2F_0 \sin \alpha A^3} \right)^{1/(3p+1)} \to 0 \qquad (58)$$

and

$$h \sim Aa^p \left[-p \frac{a^2 - y^2}{2a^2} + 1 - \frac{|y|^p}{a^p} \right] \qquad (59)$$

in $0 < \alpha < \pi$ when $p < 2$, but not when $p > 2$; this solution is always physically realisable.

In the special case $p = 2$ from (21)–(23), (A.1) and (A.2) we have

$$a \sim \left[\frac{243243\bar{Q}}{32 \sin \alpha \cos^3 \alpha A^3} \right]^{1/13} \to 0 \qquad (60)$$

and

$$h \sim \frac{\cos \alpha A}{12} \left[\frac{243243\bar{Q}}{32 \sin \alpha \cos^3 \alpha A^3} \right]^{4/13} \left(1 - \frac{y^2}{a^2} \right)^2 \qquad (61)$$

as $A^3/\bar{Q} \to \infty$ in $0 < \alpha < \pi/2$, but not in $\pi/2 \le \alpha < \pi$; this solution is also always physically realisable.

In particular, (58)–(61) show that, whatever the value of p, the rivulet becomes vanishingly narrow and infinitely deep in the limit of a strongly concave substrate $A \to \infty$, but vanishingly narrow and thin in the limit of a small volume flux $\bar{Q} \to 0^+$.

10 The Limit $A^3/\bar{Q} \to -\infty$

In the limit $A^3/\bar{Q} \to -\infty$, corresponding to a strongly convex substrate and/or a small volume flux down a convex substrate, the asymptotic behaviour is analogous to that in the limit $A^3/\bar{Q} \to \infty$ described in the previous section.

In the general case $p \neq 2$ there is a solution that is never physically realisable in which a is given by (57) and h is given by (37) as $A^3/\bar{Q} \to -\infty$ in $\pi/2 < \alpha < \pi$ when $p < 2$ and in $0 < \alpha < \pi/2$ when $p > 2$, but not otherwise, and a physically realisable solution in which a is given by (58) and h is given by (59) in $0 < \alpha < \pi$ when $p > 2$, but not when $p < 2$.

In the special case $p = 2$ there is a physically realisable solution in which a is given by (60) and h is given by (61) as $A^3/\bar{Q} \to -\infty$ in $\pi/2 < \alpha < \pi$, but not in $0 < \alpha \leq \pi/2$.

In particular, these results show that, whatever the value of p, the rivulet becomes vanishingly narrow and infinitely deep in the limit of a strongly convex substrate $A \to -\infty$, but vanishingly narrow and thin in the limit of a small volume flux $\bar{Q} \to 0^+$.

In particular, in this limit we recover Kuibin's (1996) solution for the unidirectional flow of a narrow rivulet down the underside of a circular pipe (i.e. the present solution when $\pi/2 < \alpha < \pi$ in the case $p = 2$ in the limit $A^3/\bar{Q} \to -\infty$) given by equations (60) and (61). Specifically, if we write $A = -1/2R$ (where R is a non-dimensional measure of the radius of the pipe) then from (60) the (total) width of the rivulet is given by

$$2a \sim 2 \left[\frac{243243 \bar{Q} R^3}{4 \sin \alpha |\cos \alpha|^3} \right]^{1/13} \simeq 4.666900 \left[\frac{\bar{Q} R^3}{\sin \alpha |\cos \alpha|^3} \right]^{1/13} \to 0, \tag{62}$$

from (61) the maximum thickness of the rivulet is given by

$$h(0) \sim \frac{|\cos \alpha|}{24R} \left[\frac{243243 \bar{Q} R^3}{4 \sin \alpha |\cos \alpha|^3} \right]^{4/13} \simeq 1.235329 \frac{|\cos \alpha|}{R} \left[\frac{\bar{Q} R^3}{\sin \alpha |\cos \alpha|^3} \right]^{4/13}, \tag{63}$$

and the cross-sectional area of the rivulet is given by

$$2 \int_0^a h \, dy \sim \frac{2|\cos \alpha|}{45R} \left[\frac{243243 \bar{Q} R^3}{4 \sin \alpha |\cos \alpha|^3} \right]^{5/13} \simeq 3.074751 \frac{|\cos \alpha|}{R} \left[\frac{\bar{Q} R^3}{\sin \alpha |\cos \alpha|^3} \right]^{5/13} \tag{64}$$

as $\bar{Q} R^3 \to 0$, in agreement with Kuibin's (1996) equations (21), (19) and (20), respectively. Note that, since Kuibin (1996) considered only unidirectional flow (with α constant), he incorporated a factor of $|\cos \alpha|^{-1/2}$ into his characteristic length scale and a factor of $\sin \alpha/|\cos \alpha|$ into his characteristic velocity scale.

24

11 Conclusions

In this paper we used the lubrication approximation to investigate the steady locally unidirectional gravity-driven draining of a thin rivulet of a perfectly wetting Newtonian fluid down both a locally planar and a locally non-planar slowly varying substrate. In particular, we showed that the behaviour of a rivulet of perfectly wetting fluid is qualitatively different from that of a rivulet of a non-perfectly wetting fluid described by Duffy & Moffatt (1995) and Wilson & Duffy (1998).

In the case of a locally planar substrate ($H \equiv 0$) we found that there are no rivulets possible in $0 \le \alpha \le \pi/2$ (i.e. there are no sessile rivulets or rivulets on a vertical substrate), but that there are infinitely many pendent rivulets running continuously from $\alpha = \pi/2$ (where they become infinitely wide and vanishingly thin according to (16) as $\alpha \to \pi/2^+$) to $\alpha = \pi$ (where they become infinitely deep with finite semi-width $n\pi$ according to (17) as $\alpha \to \pi^-$). This behaviour is qualitatively different from the corresponding behaviour in the non-perfectly wetting case, in which, in particular, there is always a rivulet running continuously from $\alpha = 0$ to $\alpha = \pi$, and the higher-branch solutions in $\pi/2 < \alpha \le \pi$ are not physically realisable. This qualitative difference in behaviour can be understood by examining the solution in the non-perfectly wetting case obtained by Duffy & Moffatt (1995) and Wilson & Duffy (1998, Section V) in the limit of small contact angle. Specifically if we write the contact angle in the non-perfectly wetting case as $\beta = \epsilon \beta^*$ and let $\beta^* \to 0$ then using the present non-dimensionalisation we find that in $0 \le \alpha \le \pi/2$ the rivulet becomes infinitely wide and vanishingly thin according to

$$a \sim \frac{3\bar{Q}m^3}{2\beta^3 \sin \alpha} \to \infty, \quad h_{\mathrm{m}} \sim \frac{\beta}{m} \to 0 \tag{65}$$

when $0 \le \alpha < \pi/2$ and

$$a \sim \left(\frac{105\bar{Q}}{4\beta^3 \sin \alpha} \right)^{1/4} \to \infty, \quad h_{\mathrm{m}} \sim \frac{1}{2} \left(\frac{105\beta\bar{Q}}{4 \sin \alpha} \right)^{1/4} \to 0 \tag{66}$$

25

when $\alpha = \pi/2$, but in $\pi/2 < \alpha \le \pi$ the rivulet has finite width and thickness given by

$$a \sim \frac{\pi}{m} - \frac{1}{m^2} \left(\frac{5\pi\beta^3 \sin\alpha}{3Qm} \right)^{1/3}, \qquad h_{\mathrm{m}} \sim \left(\frac{24Qm}{5\pi \sin\alpha} \right)^{1/3}, \qquad (67)$$

in agreement with the solution in the perfectly wetting case described in section 3.

In the case of a locally non-planar substrate ($H \not\equiv 0$) with a power-law transverse profile in the form $H = A|y|^p$ for $p > 0$ we found, rather unexpectedly, that the behaviour of the possible lowest-branch rivulets (i.e. those satisfying $0 \le a \le \pi/m$ in $\pi/2 < \alpha \le \pi$) is qualitatively different in the cases $p < 2$, $p = 2$ and $p > 2$ as well as in the cases of locally concave ($A > 0$) and locally convex ($A < 0$) substrates.

In the case of a locally concave substrate (i.e. when $A > 0$) there is always a solution near $\alpha = 0$ representing a rivulet that becomes infinitely wide and deep according to (24) and (25) as $\alpha \to 0^+$. When $p < 2$ the rivulet runs continuously through $\alpha = \pi/2$ to $\alpha = \alpha_{\mathrm{max}}$ ($\pi/2 < \alpha_{\mathrm{max}} < \pi$) where it fails to be physically realisable via $h''(a) = 0$. In the special case of a locally parabolic substrate ($p = 2$) the rivulet runs continuously to $\alpha = \pi/2$ where it becomes infinitely wide and vanishingly thin according to (33) and (34) as $\alpha \to \pi/2^-$. When $p > 2$ the rivulet runs continuously to $\alpha = \alpha^*$ ($0 < \alpha^* < \pi/2$) where it fails to be physically realisable via $h(0) = 0$.

On the other hand, in the case of a locally convex substrate (i.e. when $A < 0$) there is always a solution near $\alpha = \pi$ representing a rivulet that becomes infinitely deep with semi-width π according to (38) and (39) with $n = 1$ as $\alpha \to \pi^-$. When $p < 2$ the rivulet runs continuously from $\alpha = \alpha^*$ ($\pi/2 < \alpha^* < \pi$) where it fails to be physically realisable via $h(0) = 0$. In the special case of a locally parabolic substrate ($p = 2$) the rivulet runs continuously from $\alpha = \pi/2$ where it becomes infinitely wide and vanishingly thin according to (33) and (34) as $\alpha \to \pi/2^+$. When $p > 2$ the rivulet runs continuously from $\alpha = \alpha_{\mathrm{min}}$ ($0 < \alpha_{\mathrm{min}} < \pi/2$) where it fails to be physically realisable via $h''(a) = 0$, through $\alpha = \pi/2$.

We also determined the behaviour of the solutions in the physically important limits $A \to 0$,

26

$A \to \infty$, $A \to -\infty$, $\bar{Q} \to 0^+$, and $\bar{Q} \to \infty$. In particular, we showed that, as expected, the solution in the case of a locally planar substrate is recovered at leading order in the limit $A \to 0$, and that Kuibin's (1996) solution for the unidirectional flow of a narrow rivulet down the underside of a circular pipe is recovered when $\pi/2 < \alpha < \pi$ in the case $p = 2$ in the limit $A^3/\bar{Q} \to -\infty$.

It is interesting to compare the behaviour described above with the behaviour in the non-perfectly wetting case. In the two cases the behaviour near the top of the cylinder is qualitatively the same (i.e. in both cases there is always a solution near $\alpha = 0$ when $A > 0$ but not when $A < 0$) but the behaviour near the bottom of the cylinder is rather different. Specifically in the non-perfectly wetting case there is a positive critical value of A, denoted by $A_c > 0$, such that if $A < A_c$ then there is a solution near $\alpha = \pi$, and so if $0 < A < A_c$ then there is a rivulet running continuously from $\alpha = 0$ to $\alpha = \pi$. If we again write the contact angle in the non-perfectly wetting case as $\beta = \epsilon\beta^*$ then using the present non-dimensionalisation Wilson & Duffy's (1998, Equation 38) expression for A_c in the non-perfectly wetting case $\beta \neq 0$ becomes

$$A_c = \frac{\beta}{p(n\pi)^{p-1}} \tag{68}$$

and thus, in particular, $A_c \to 0$ as $\beta \to 0$, which is entirely consistent with the present results in the perfectly wetting case $\beta = 0$. A notable difference between the behaviour in the two cases is that, in sharp contrast to the present results, there is, in general, *nothing* special about the case of a locally parabolic substrate $p = 2$ in the non-perfectly wetting case.

Although a full stability analysis of the present rivulet solutions is outside the scope of the present work, a quasi-static stability analysis similar to that undertaken by Wilson & Duffy (1998) in the non-perfectly wetting case indicates that the present physically realisable solutions are quasi-statically stable provided that the flow remains symmetric and unidirectional.

Acknowledgement

Appendix A : Asymptotic Behaviour of the Functions f and F

For future reference we note the following asymptotic results for the functions f and hence F, defined by equations (19) and (23), respectively.

In the limit $M \to 0$ we have

$$f = \frac{1 - Y^2}{2} - \frac{(1 - Y^2)^2}{24} SM^2 + O(M^4) \tag{A.1}$$

and hence

$$F \sim \begin{cases} (F_0 + F_1 SM^2)M^{3p+1} \to 0 & \text{if } p \neq 2, \\ \dfrac{16}{81081} SM^{13} \to 0 & \text{if } p = 2, \end{cases} \tag{A.2}$$

where we have defined

$$F_0 = -\frac{2p^3(p-2)^3(12p^3 + 124p^2 + 403p + 361)}{35(p+1)(p+3)(p+5)(2p+1)(3p+1)(2p+3)}, \tag{A.3}$$

$$F_1 = \frac{2p^3(p-2)^2(16p^5 + 320p^4 + 2444p^3 + 8938p^2 + 15180p + 9327)}{315(p+1)(p+3)(p+5)(p+7)(2p+1)(2p+3)(2p+5)}. \tag{A.4}$$

If $M \to \infty$ in $\cos\alpha > 0$ then

$$f \sim \frac{1}{M}\left[1 - e^{-M(1-|Y|)}\right] \to 0 \tag{A.5}$$

and hence

$$F \sim \frac{6p^3 M^{3p+1}}{(p+1)(2p+1)(3p+1)} \to \infty. \tag{A.6}$$

If $M \to n\pi$ $(n = 1, 2, 3, \ldots)$ in $\cos\alpha < 0$ then

$$f \sim \frac{1 - (-1)^n \cos n\pi Y}{n\pi(n\pi - M)} \to \begin{cases} -\infty & \text{when } M \to n\pi^+, \\ +\infty & \text{when } M \to n\pi^- \end{cases} \tag{A.7}$$

and hence

$$F \sim -\frac{5p^3(n\pi)^{3p-2}}{2(n\pi - M)^3} \to \begin{cases} +\infty & \text{when } M \to n\pi^+, \\ -\infty & \text{when } M \to n\pi^-. \end{cases} \tag{A.8}$$

Appendix B : Details of the Numerical Procedure

Although it is, in principle, straightforward to solve the equation $Q = \bar{Q}$ numerically by means of a root-finding algorithm to obtain a as a function of α, in practice this calculation can not only require a very accurate initial guess for the iterative numerical procedure but can also be rather time-consuming. To obtain the numerical results presented in the present work we instead adopted the quicker and more efficient method described below. Differentiating the equation $Q = \bar{Q}$ (with Q given by (11), and with $\bar{Q}$ a prescribed constant) yields

$$Q_\alpha + Q_a \frac{\mathrm{d}a}{\mathrm{d}\alpha} = 0, \tag{B.1}$$

and we regard this as a first-order differential equation for $a(\alpha)$. In the simplest cases (B.1) is easily solved by a shooting method, subject to an appropriate initial condition of the form $a(\alpha_0) = a_0$ (obtained by solving $Q = \bar{Q}$ with $\alpha = \alpha_0$). In more complicated cases a is a multi-valued function of α; in such cases we represent the solution parametrically in the form $\alpha = \alpha(s)$, $a = a(s)$, in terms of a parameter s that varies along the solution curve. Then we differentiate $Q = \bar{Q}$ with respect to s to obtain

$$Q_\alpha \frac{\mathrm{d}\alpha}{\mathrm{d}s} + Q_a \frac{\mathrm{d}a}{\mathrm{d}s} = 0, \tag{B.2}$$

and so we may write

$$\frac{\mathrm{d}\alpha}{\mathrm{d}s} = \frac{Q_a}{(Q_\alpha^2 + Q_a^2)^{1/2}}, \quad \frac{\mathrm{d}a}{\mathrm{d}s} = -\frac{Q_\alpha}{(Q_\alpha^2 + Q_a^2)^{1/2}}, \tag{B.3}$$

which we regard as a pair of first-order differential equations for $\alpha(s)$ and $a(s)$ which are again easily solved by a shooting method subject to appropriate initial conditions of the form $\alpha(0) = \alpha_0$, $a(0) = a_0$.

References

[1] Alekseenko, S. V., Geshev, P. I. & Kuibin, P. A. (1997) Free-boundary fluid flow on an inclined cylinder. *Physics - Doklady* **42**, 269–272. [Translated from *Doklady Akademii Nauk* **354**, 47–50 (1997).]

[2] Allen, R. F. & Biggin, C. M. (1974) Longitudinal flow of a lenticular liquid filament down an inclined plane. *Phys. Fluids* **17**, 287–291.

[3] Davis, S. H. (1980) Moving contact lines and rivulet instabilities. Part 1. The static rivulet. *J. Fluid Mech.* **98**, 225–242.

[4] Duffy, B. R. & Moffatt, H. K. (1995) Flow of a viscous trickle on a slowly varying incline. *Chem. Engng J.* **60**, 141–146.

[5] Duffy, B. R. & Wilson, S. K. (2003) A rivulet of perfectly wetting fluid with temperature-dependent viscosity draining down a uniformly heated or cooled slowly varying substrate. *Phys. Fluids* **15**, 3236–3239.

[6] Hansen, E. B. & Solonnikov, V. A. (1990) An existence theorem for Poiseuille flow with surface tension in an open channel. *Math. Meth. Appl. Sci.* **13**, 23–30.

[7] Kuibin, P. A. (1996) An asymptotic description of the rivulet flow along an inclined cylinder. *Russ. J. Engng Thermophys.* **6**, 33–45.

[8] Kuo, Y. & Tanner, R. I. (1972) Laminar Newtonian flow in open channels with surface tension. *Int. J. Mech. Sci.* **14**, 861–873.

[9] Schmuki, P. & Laso, M. (1990) On the stability of rivulet flow. *J. Fluid Mech.* **215**, 125–143.

[10] Towell, G. D. & Rothfeld, L. B. (1966) Hydrodynamics of rivulet flow. *AIChE J.* **12**, 972–980.

[11] Weiland, R. H. & Davis, S. H. (1981) Moving contact lines and rivulet instabilities. Part 2. Long waves on flat rivulets. *J. Fluid Mech.* **107**, 261–280.

[12] Wilson, S. K. & Duffy, B. R. (1998) On the gravity-driven draining of a rivulet of viscous fluid down a slowly varying substrate with variation transverse to the direction of flow. *Phys. Fluids* **10**, 13–22.

[13] Young, G. W. & Davis, S. H. (1987) Rivulet instabilities. *J. Fluid Mech.* **176**, 1–31.

Table and Table Caption

p	h_0	a_0	a_1/a_0^3
1	$\dfrac{A}{2a_0}(a_0 - |y|)^2$	$\left(\dfrac{84\bar{Q}}{A^3}\right)^{1/4}$	$\dfrac{23}{288}$
3	$-\dfrac{A}{2}(a_0 + 2|y|)(a_0 - |y|)^2$	$\left(-\dfrac{1680\bar{Q}}{43A^3}\right)^{1/10}$	$-\dfrac{2201}{28380}$
4	$-A(a_0^2 - y^2)^2$	$\left(-\dfrac{9009\bar{Q}}{2048A^3}\right)^{1/13}$	$-\dfrac{1}{26}$
5	$-\dfrac{A}{2}(2|y|^3 + 4a_0y^2 + 6a_0^2|y| + 3a_0^3)(a_0 - |y|)^2$	$\left(-\dfrac{2002\bar{Q}}{1635A^3}\right)^{1/16}$	$-\dfrac{288059}{11301120}$
6	$-A(2a_0^2 + y^2)(a_0^2 - y^2)^2$	$\left(-\dfrac{285285\bar{Q}}{575488A^3}\right)^{1/19}$	$-\dfrac{1091}{57324}$

Table 1: Solutions for h_0, a_0 and a_1/a_0^3 in the limit $\alpha \to \pi/2$ for a range of values of p. Note that there is no solution of this kind in the special case $p = 2$.

Figure Captions

Figure 1 : The geometry of the problem.

Figure 2 : (a) The semi-width of the rivulet a, and (b) the scaled maximum thickness of the rivulet $h_m/\bar{Q}^{1/3}$ plotted as functions of α/π in the case of a locally planar substrate $H \equiv 0$ for $n = 1, 2, 3, \ldots, 10$.

Figure 3 : Typical scaled lowest-branch ($n = 1$) transverse rivulet profiles $h/\bar{Q}^{1/3}$ plotted as functions of y in the case of a locally planar substrate $H \equiv 0$ for $\alpha = 11\pi/20, 12\pi/20, \ldots, 19\pi/20$.

Figure 4 : The function $F(M, p)$ given by (23) plotted as a function of M in the cases $\cos \alpha > 0$, $\cos \alpha = 0$ and $\cos \alpha < 0$ for (a) $p = 1$, (b) $p = 2$, and (c) $p = 3$.

Figure 5 : Numerically calculated values of (a) M_{max}, M_{min}, M_0 and M^*, and (b) F_{max}, F_{min} and F^* plotted as functions of p. Note that F_{max} and M_{max} are defined only for $p < 2$, while F_{min} and M_{min} are defined only for $p > 2$.

Figure 6 : Typical scaled transverse rivulet profiles $(H + h)/\bar{Q}^{1/3}$ plotted as functions of y for $\alpha = \pi/10, \pi/10^2, \ldots, \pi/10^6$ in the case $p = 2$ and $A^3/\bar{Q} = 1$.

Figure 7 : (a) Sketch of the rivulet semi-width a plotted as a function of α in the case $p < 2$. (b) The rivulet semi-width a plotted as a function of α/π for a range of values of $A/\bar{Q}^{1/3}$ in the case $p = 1$. Physically realisable solutions are denoted by thick solid lines, while solutions that are not physically realisable are denoted by thick dashed lines. The curves $\pi|\cos \alpha|^{-1/2}$ and $M_0|\cos \alpha|^{-1/2}$ in $\pi/2 < \alpha \leq \pi$ are denoted by thin dashed lines.

Figure 8 : Numerically calculated values of (a) α_{max}, α_{min} and α^*, and (b) a_{max}, a_{min} and a^* plotted as functions of $A/\bar{Q}^{1/3}$ in the cases $p = 1$ and $p = 3$. Note that α_{max} and a_{max} are

33

defined only for $A > 0$, while $\alpha_{\min}$ and $a_{\min}$ are defined only for $A < 0$.

Figure 9 : Typical scaled transverse rivulet profiles $(H + h)/\bar{Q}^{1/3}$ in the case $p = 1$ plotted as functions of y for (a) $\alpha = \pi/4$ and 0.53π (twice) when $A/\bar{Q}^{1/3} = 1$, and (b) $\alpha = 0.54\pi$, $6\pi/10$, $7\pi/10$, $8\pi/10$ and $9\pi/10$ when $A/\bar{Q}^{1/3} = -1$. Physically realisable solutions are denoted by solid lines, while solutions that are not physically realisable are denoted by dashed lines.

Figure 10 : (a) Sketch of the rivulet semi-width a plotted as a function of α in the special case $p = 2$. (b) The rivulet semi-width a plotted as a function of α/π for a range of values of $A/\bar{Q}^{1/3}$ in the special case $p = 2$. The curve $\pi|\cos\alpha|^{-1/2}$ in $\pi/2 < \alpha \leq \pi$ is denoted by a thin dashed line. Note that in this special case all the solutions are physically realisable.

Figure 11 : Typical scaled transverse rivulet profiles $(H + h)/\bar{Q}^{1/3}$ in the special case $p = 2$ plotted as functions of y for (a) $\alpha = \pi/10$, $\pi/5$, $3\pi/10$ and $2\pi/5$ when $A/\bar{Q}^{1/3} = 1$, and (b) $\alpha = 3\pi/5$, $7\pi/10$, $4\pi/5$ and $9\pi/10$ when $A/\bar{Q}^{1/3} = -1$. Note that in this special case all the solutions are physically realisable.

Figure 12 : (a) Sketch of the rivulet semi-width a plotted as a function of α in the case $p > 2$. (b) The rivulet semi-width a plotted as a function of α/π for a range of values of $A/\bar{Q}^{1/3}$ in the case $p = 3$. Physically realisable solutions are denoted by thick solid lines, while solutions that are not physically realisable are denoted by thick dashed lines. The curve $\pi|\cos\alpha|^{-1/2}$ in $\pi/2 < \alpha \leq \pi$ and the curve $M_0(\cos\alpha)^{-1/2}$ in $0 \leq \alpha < \pi/2$ are denoted by thin dashed lines.

Figure 13 : Typical scaled transverse rivulet profiles $(H + h)/\bar{Q}^{1/3}$ in the case $p = 3$ plotted as functions of y for (a) $\alpha = \pi/10$, $\pi/5$ and $3\pi/10$ when $A/\bar{Q}^{1/3} = 1$, and (b) $\alpha = 0.30\pi$ (twice) and $3\pi/4$ when $A/\bar{Q}^{1/3} = -1$. Physically realisable solutions are denoted by solid lines, while solutions that are not physically realisable are denoted by dashed lines.

MARKED PHOTOCOPIES

Fig. 1

Substrate
$z = H(y)$

Free surface
$z = (H+h)(y)$

α

$\underset{\sim}{g}$

Edge of
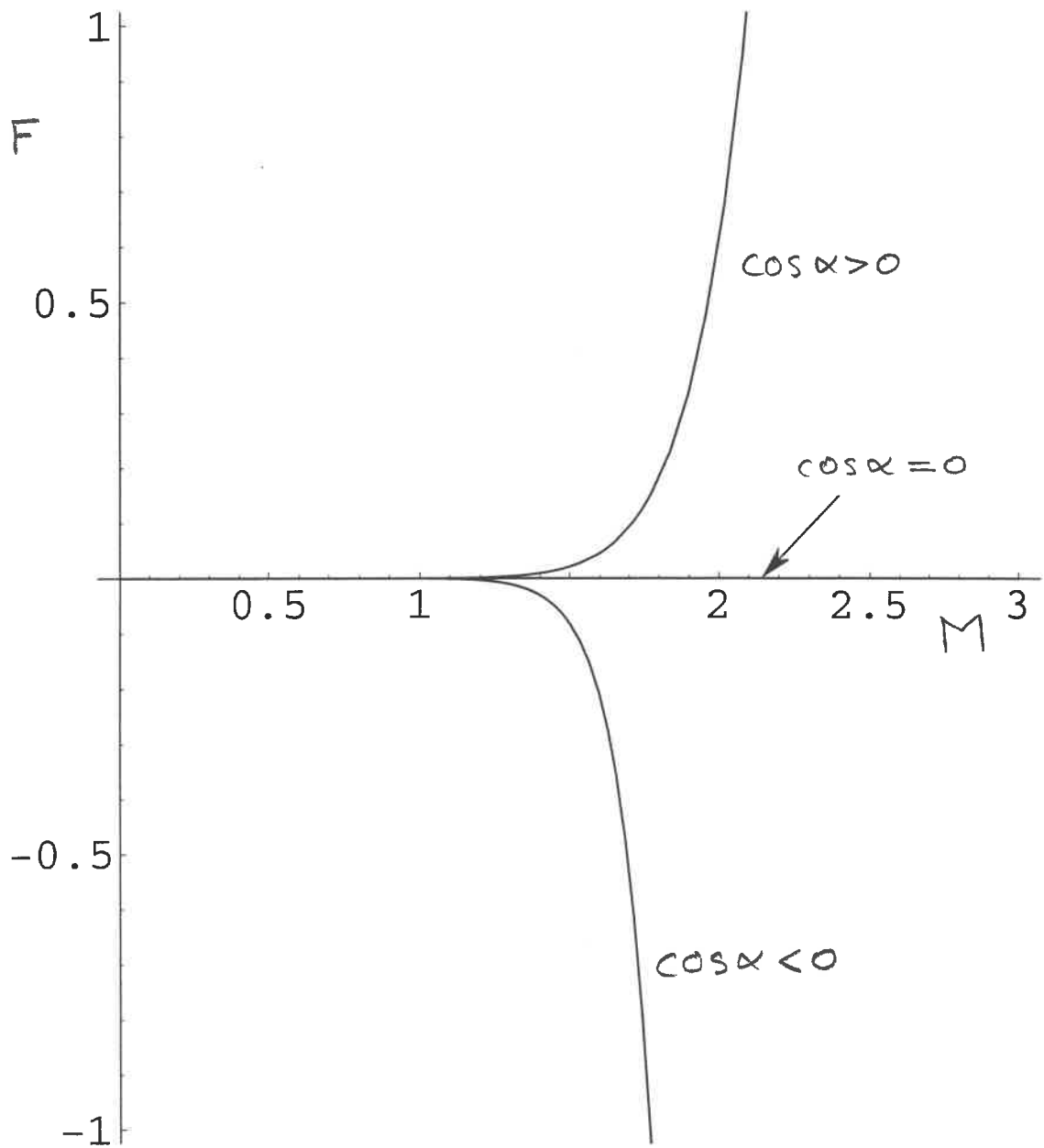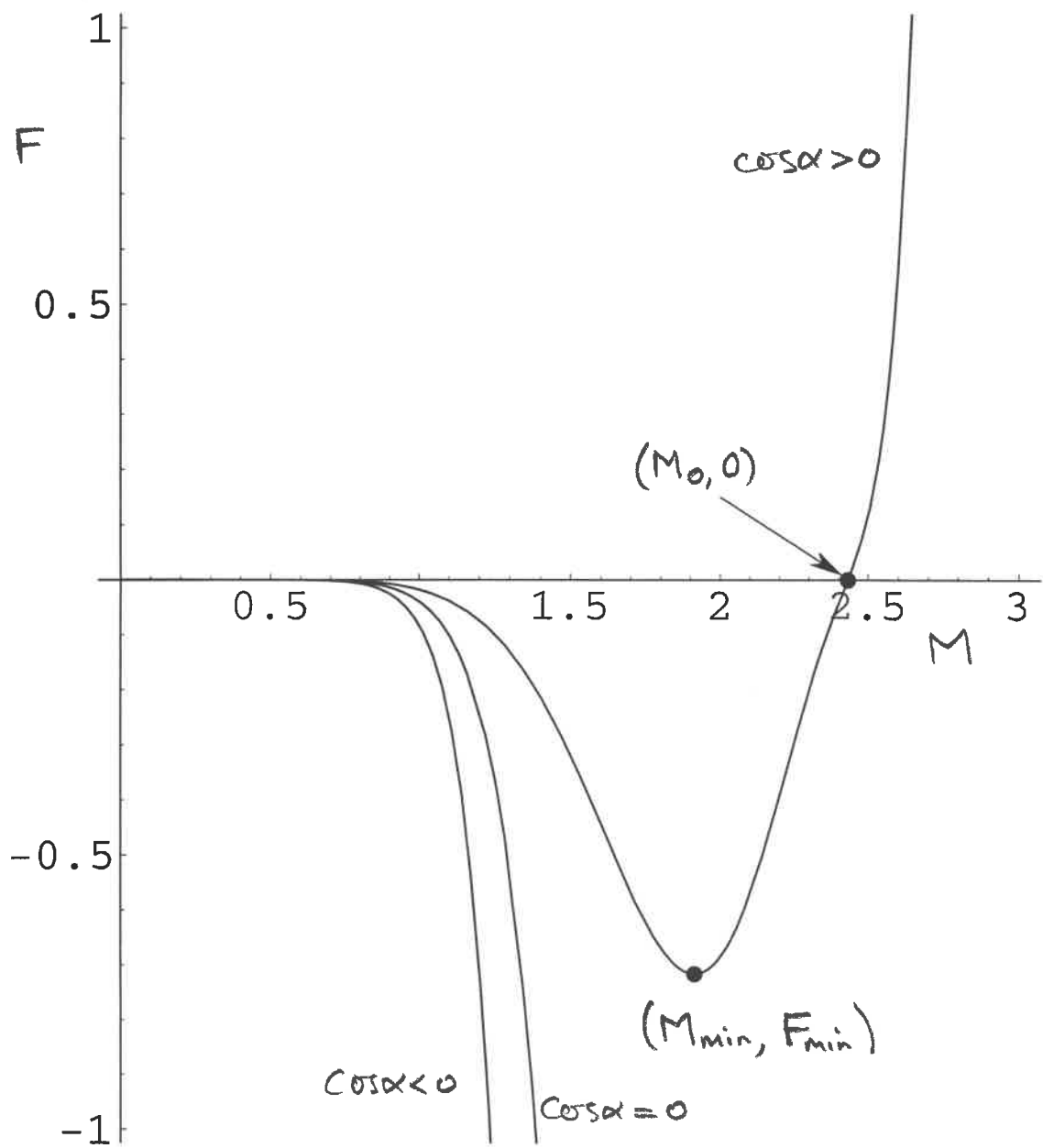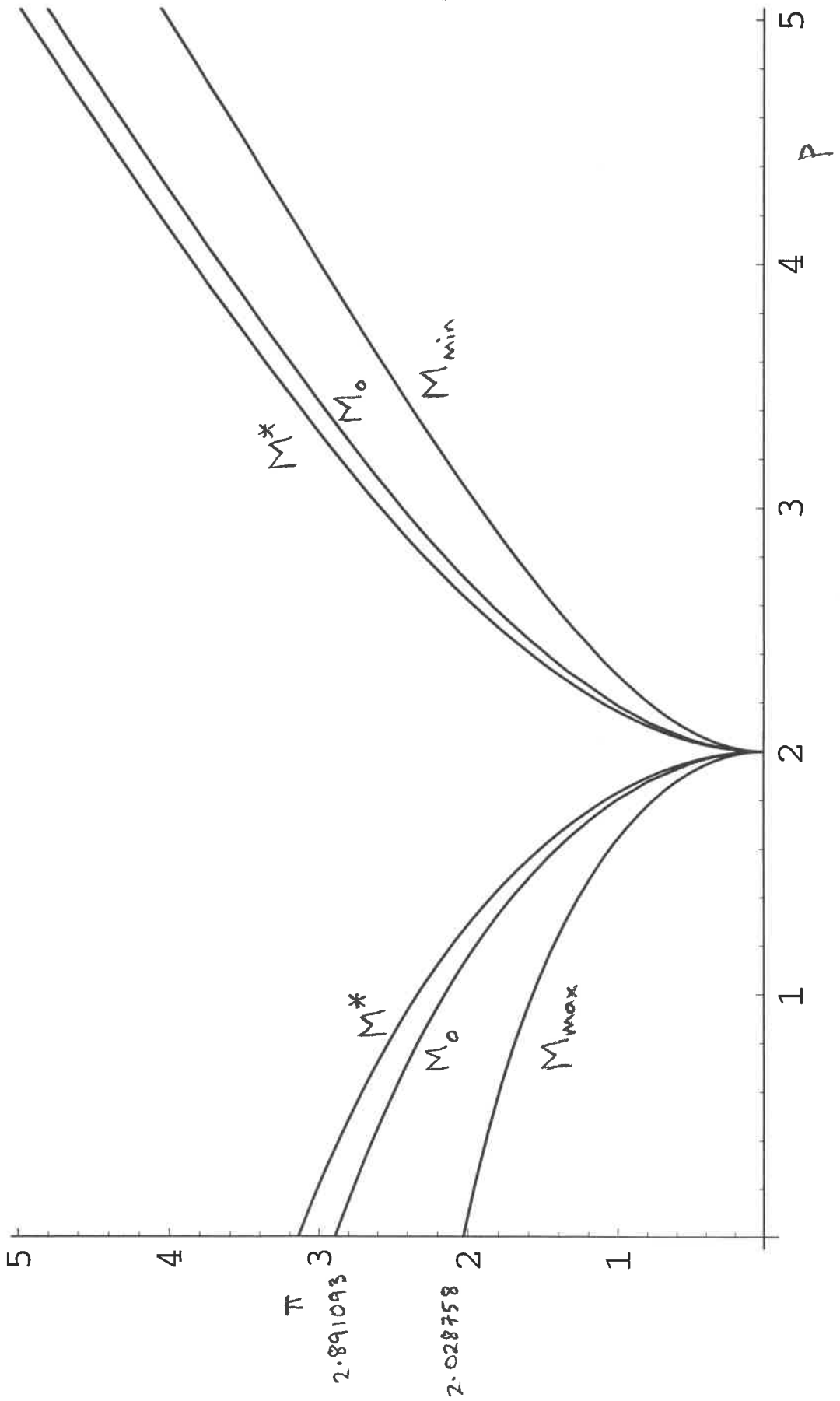rivulet
$y = a$

y

x
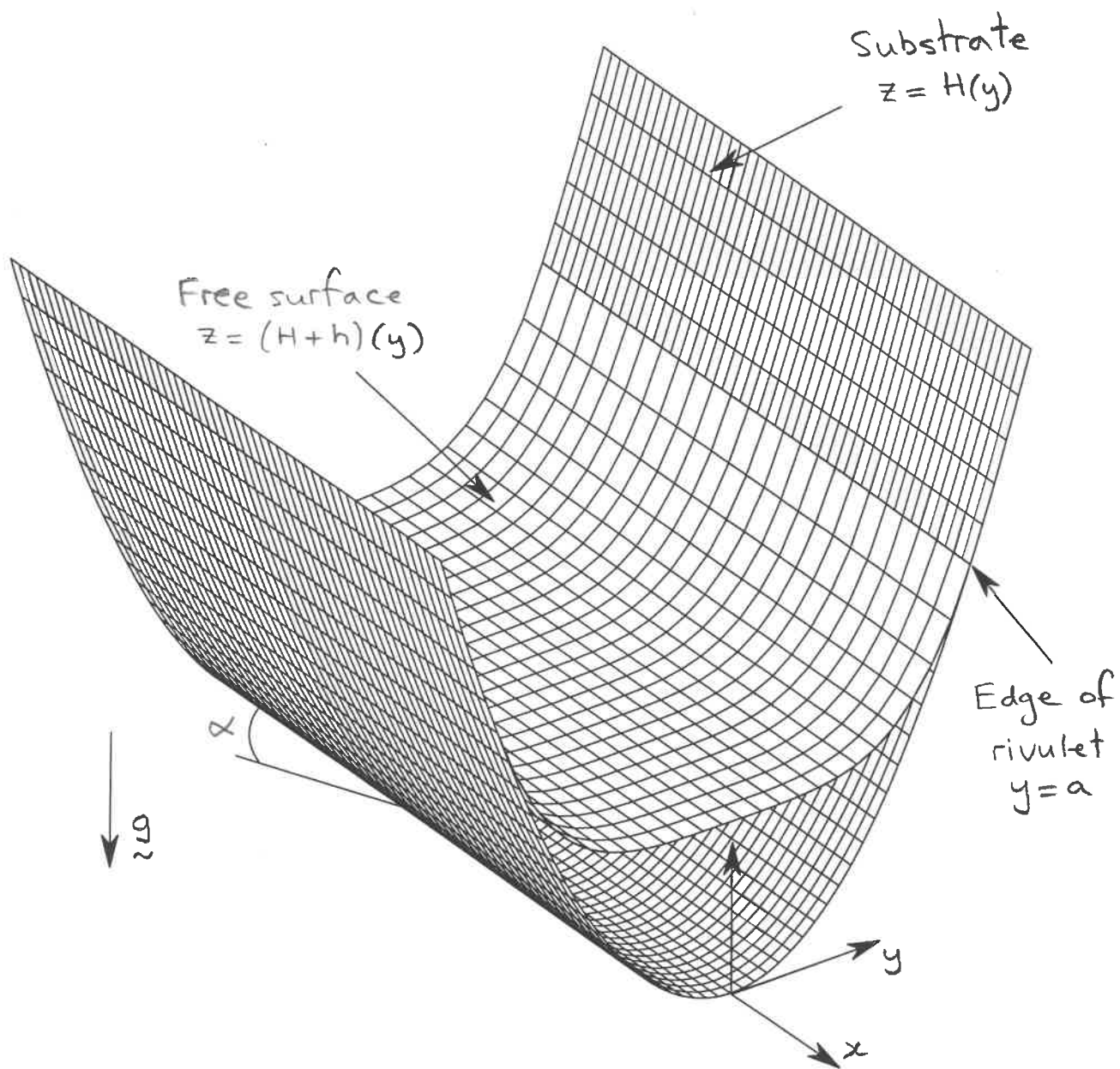
Fig. 2(a)
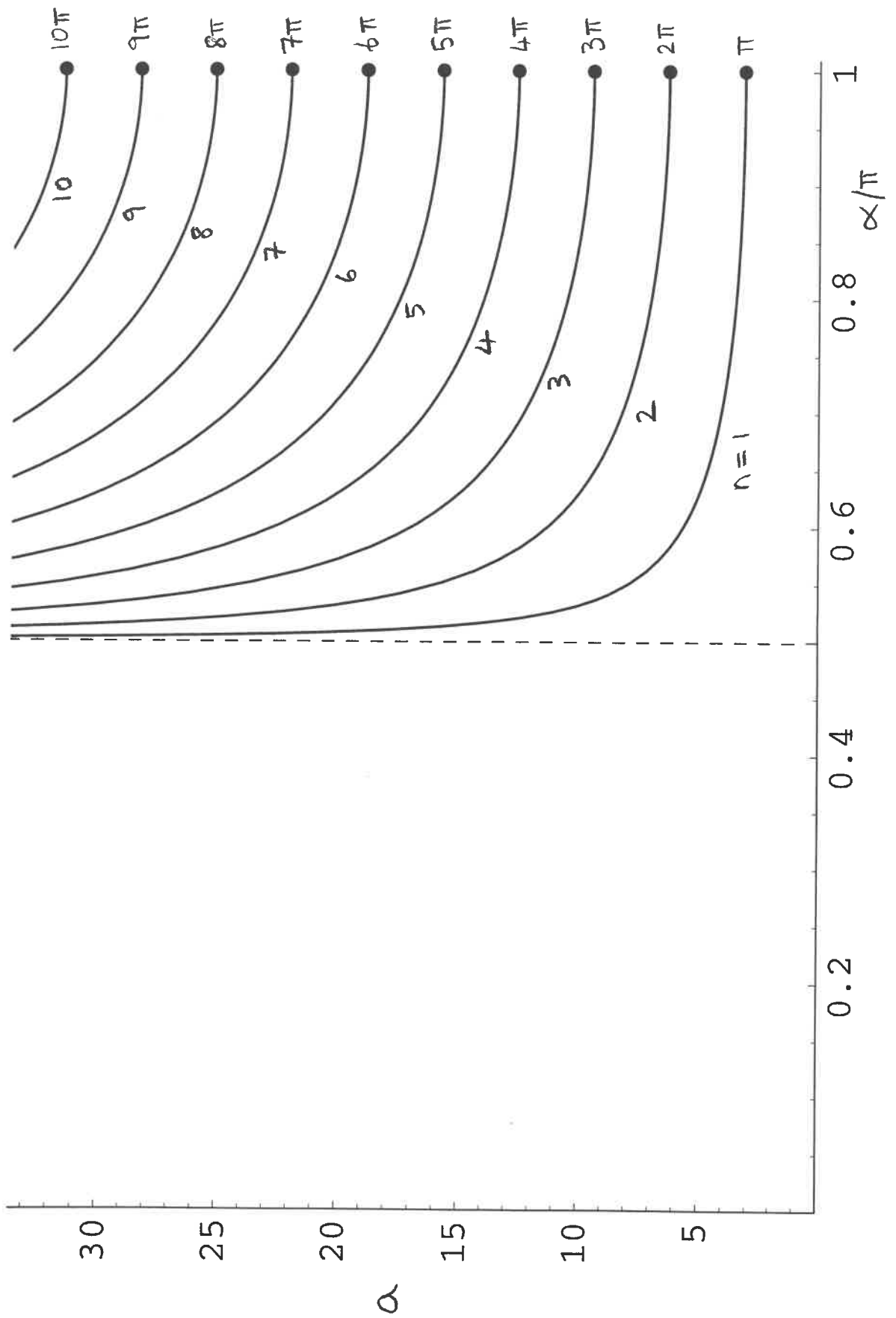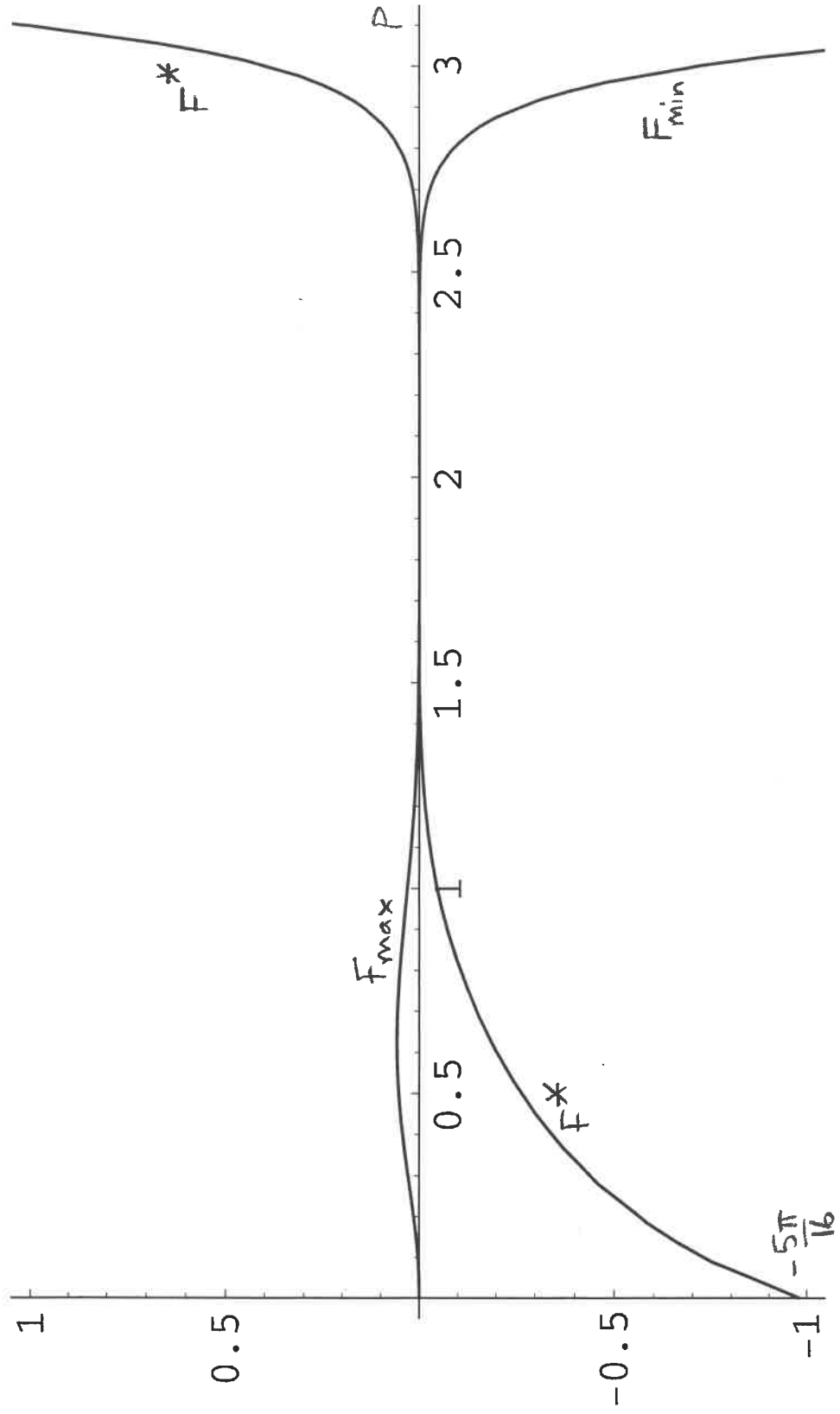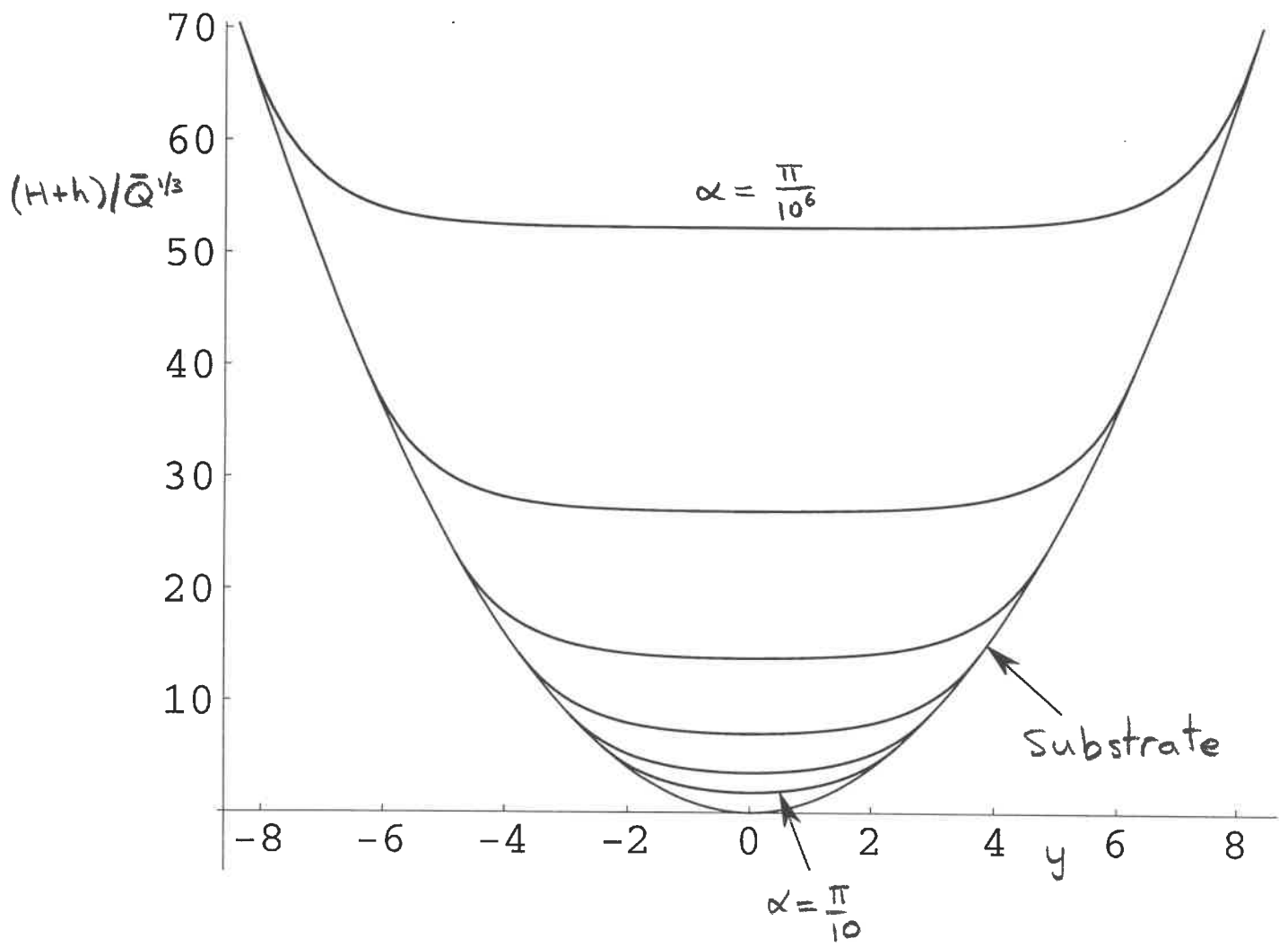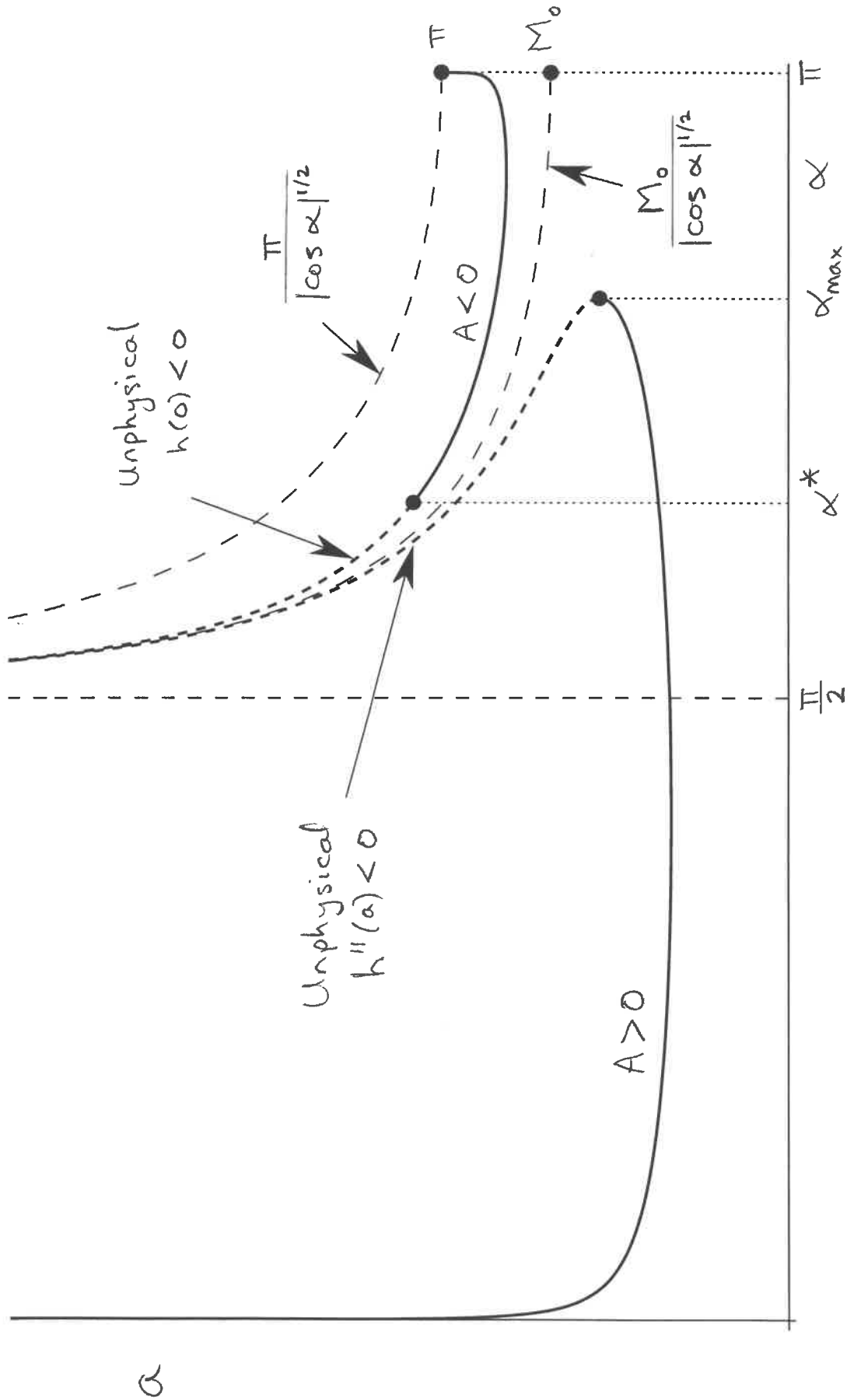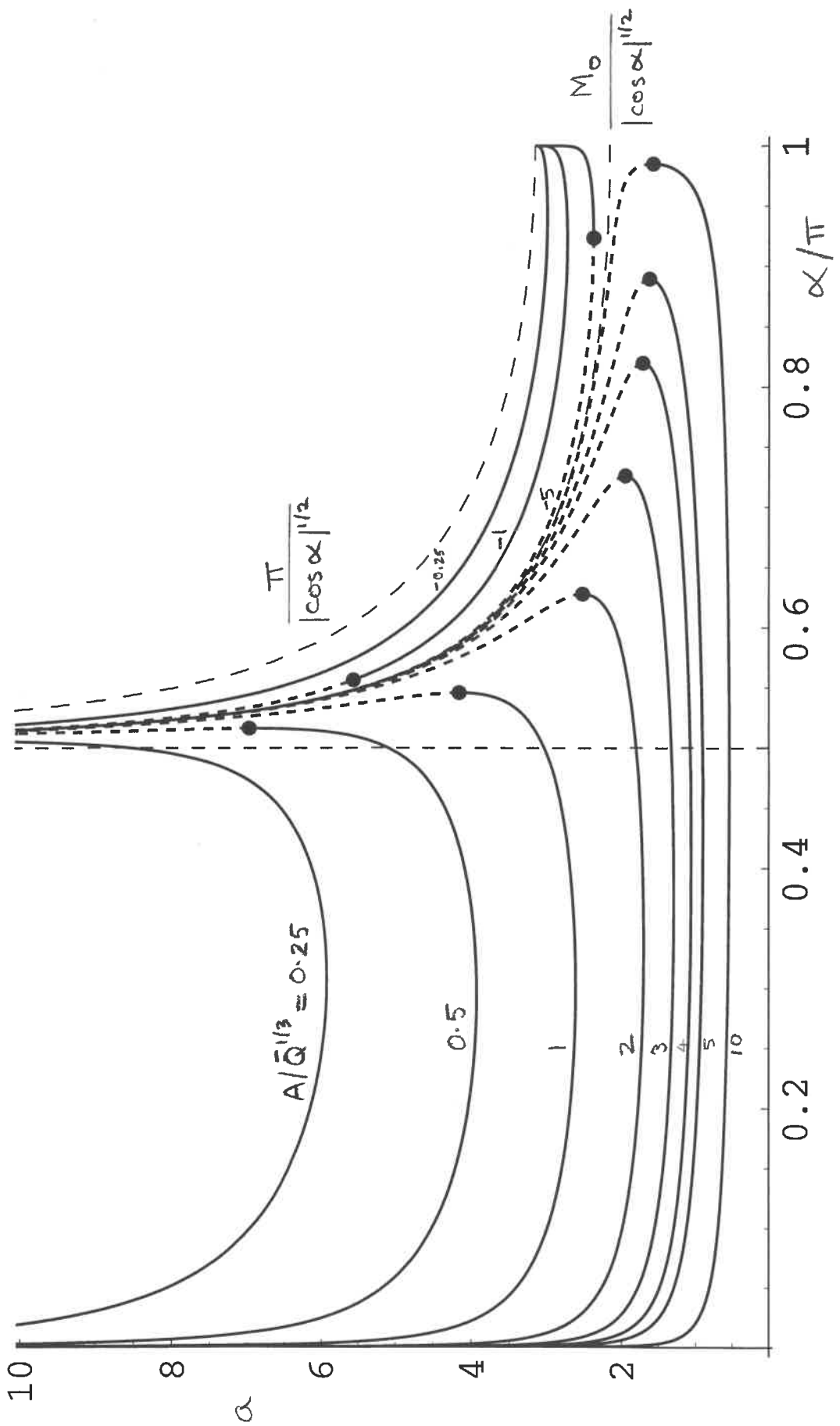
Fig. 2(b)
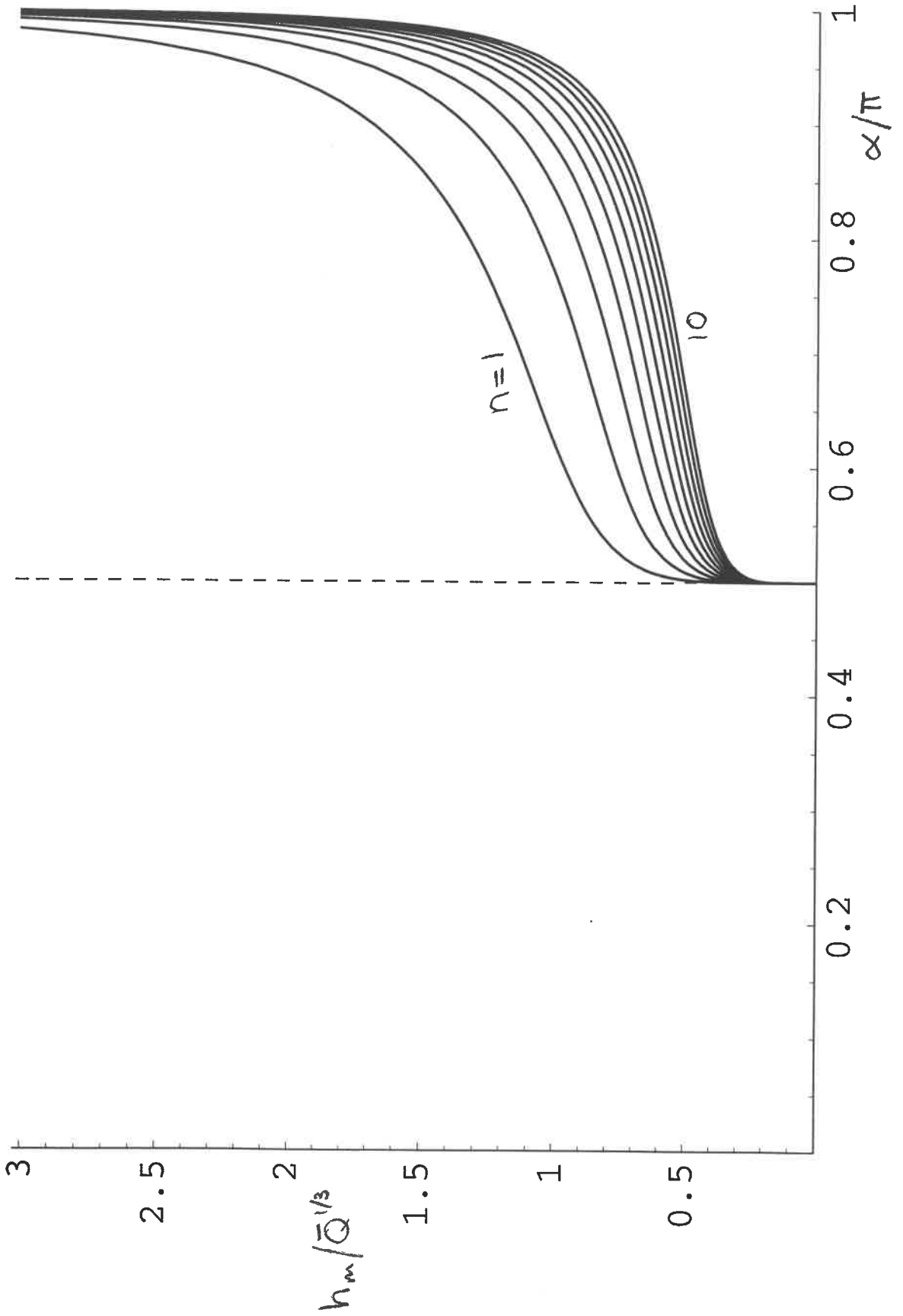
Fig 3
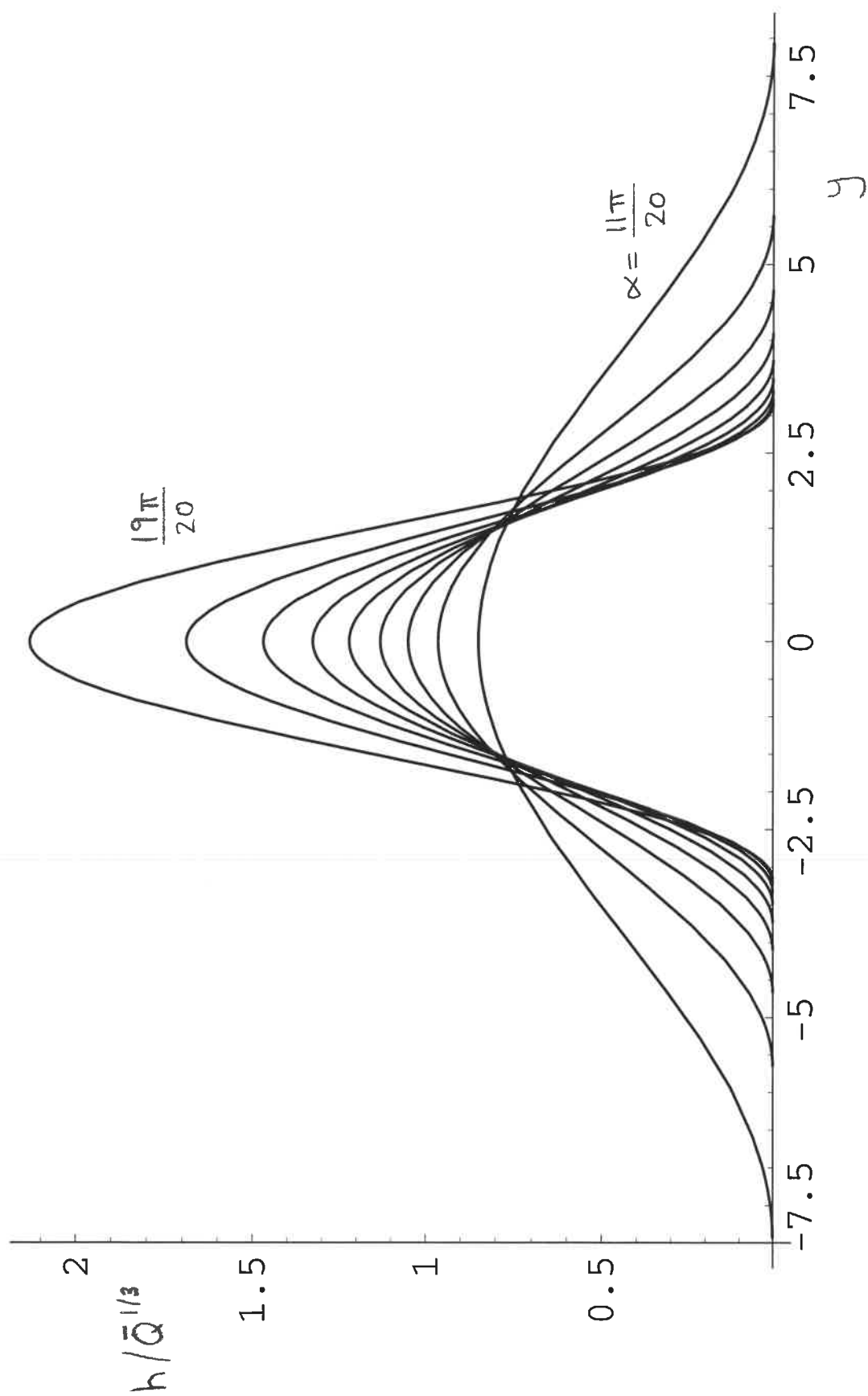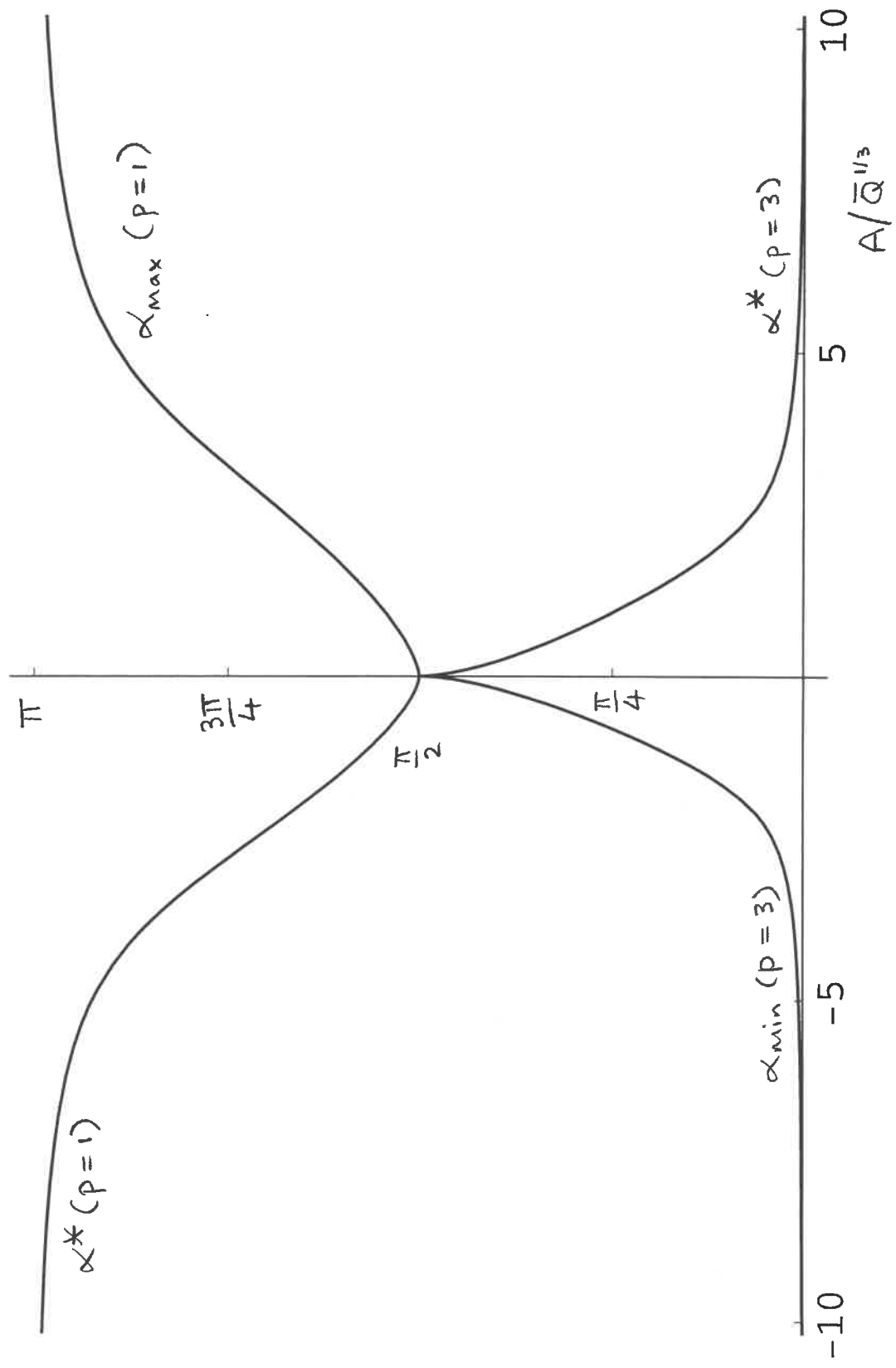
Fig. 4(a)
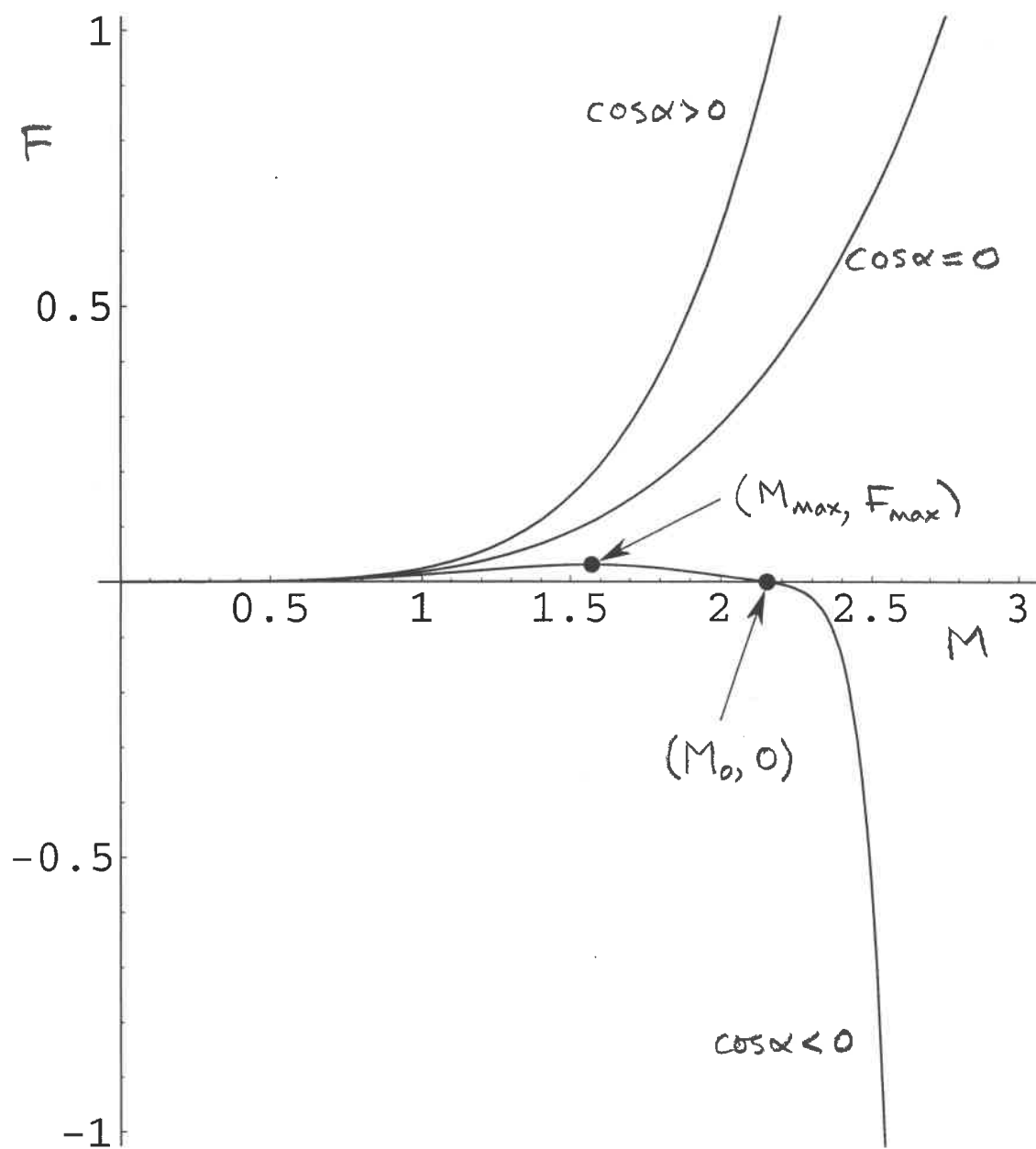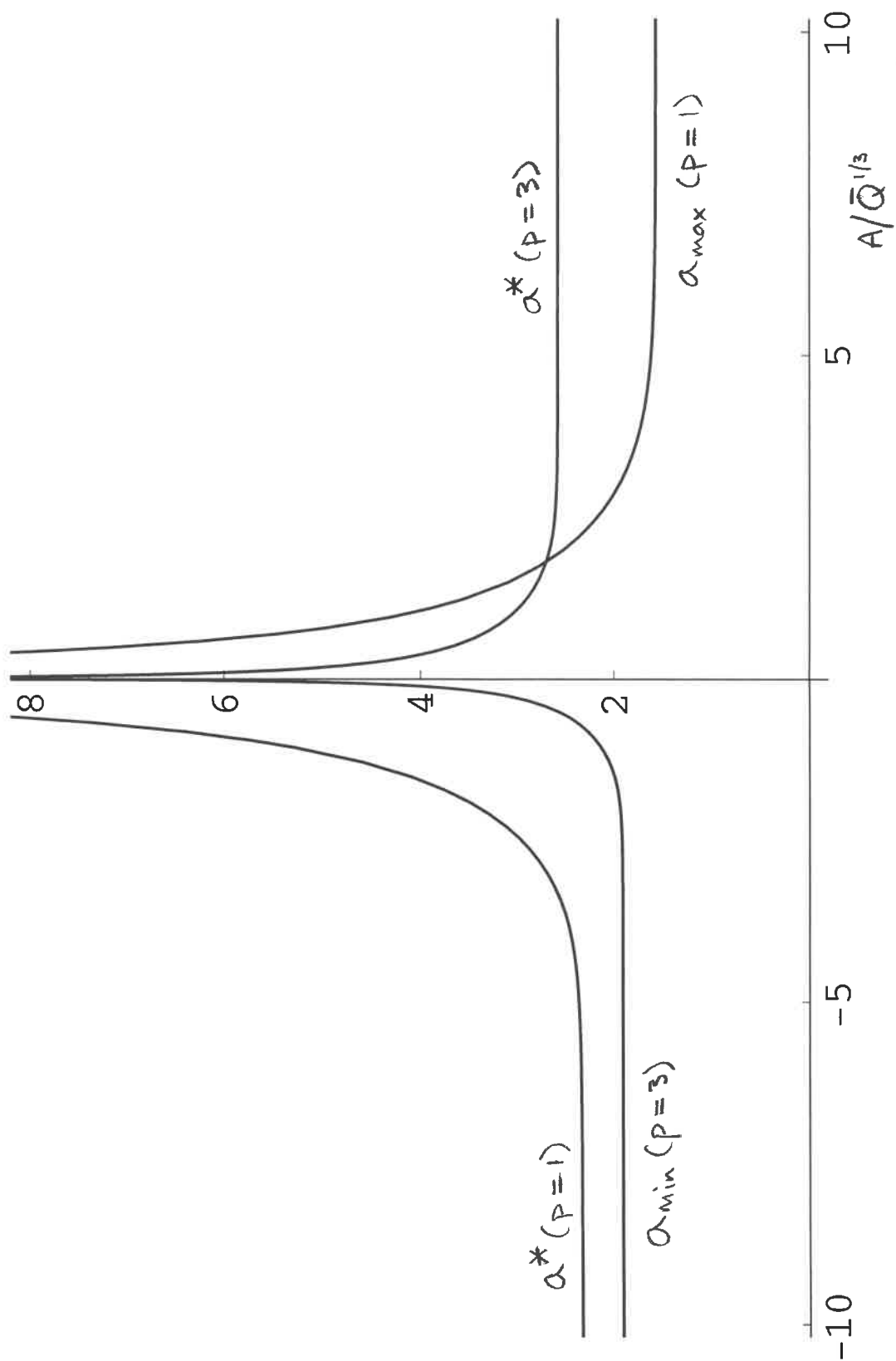
Fig. 4(b)
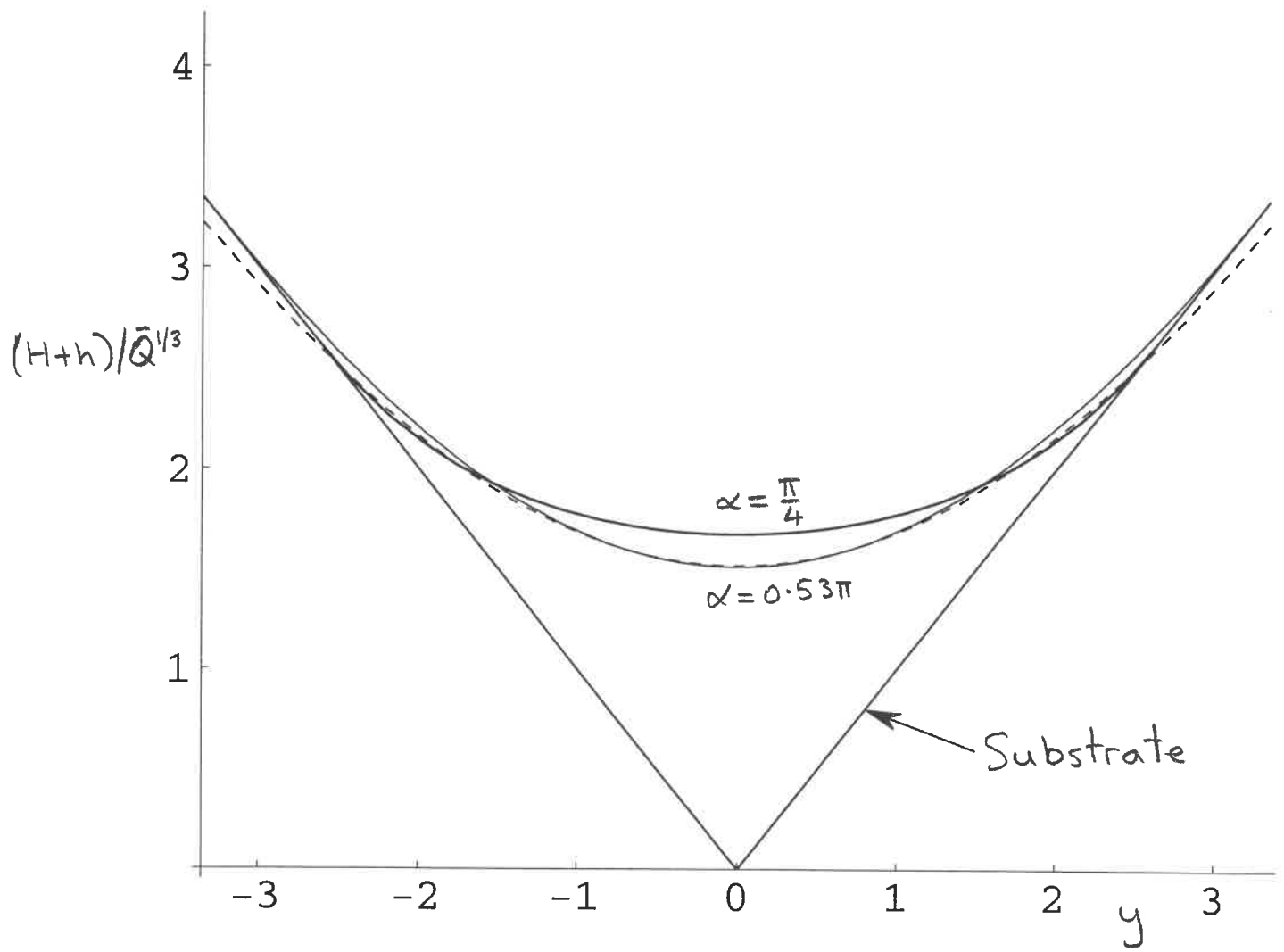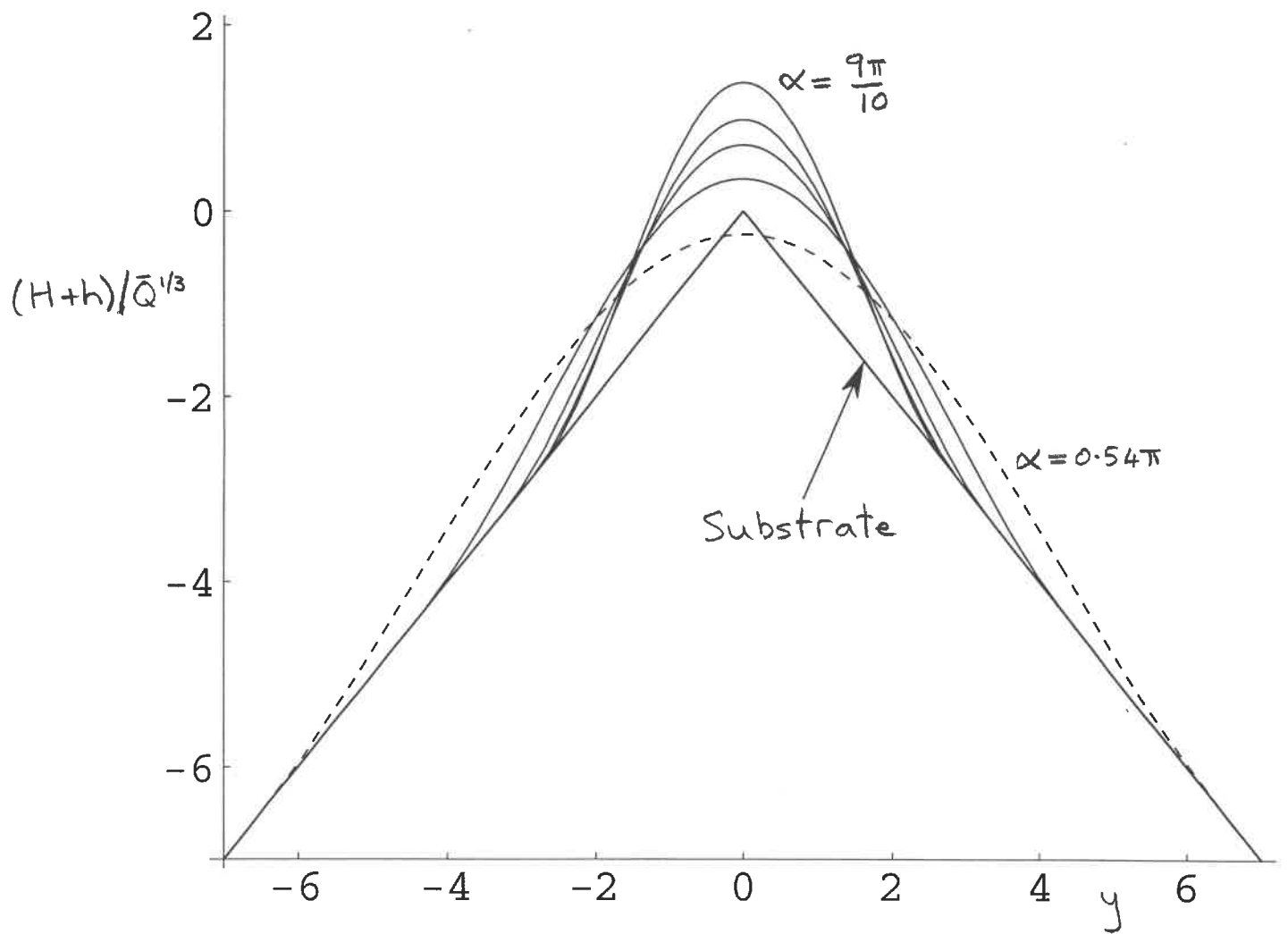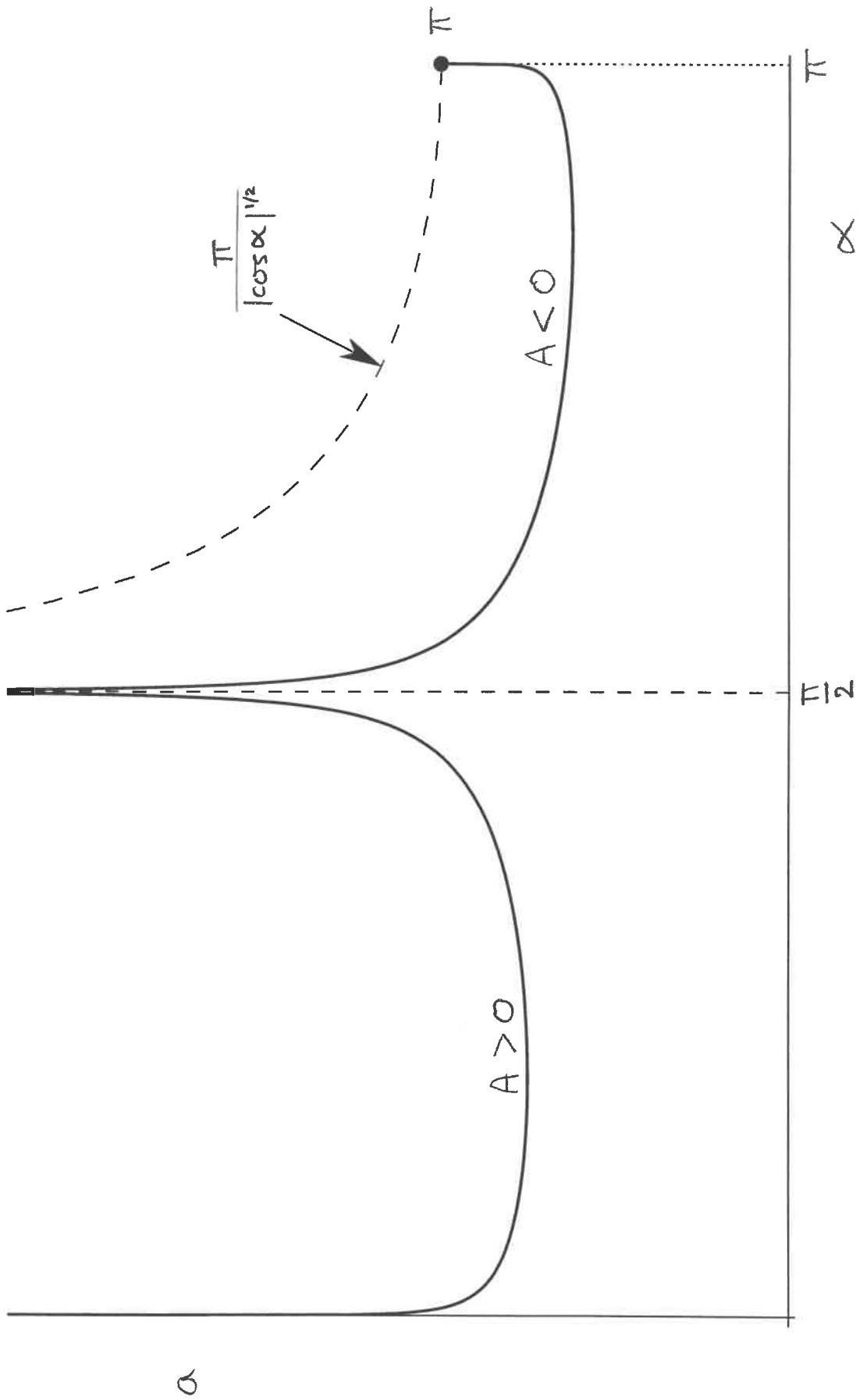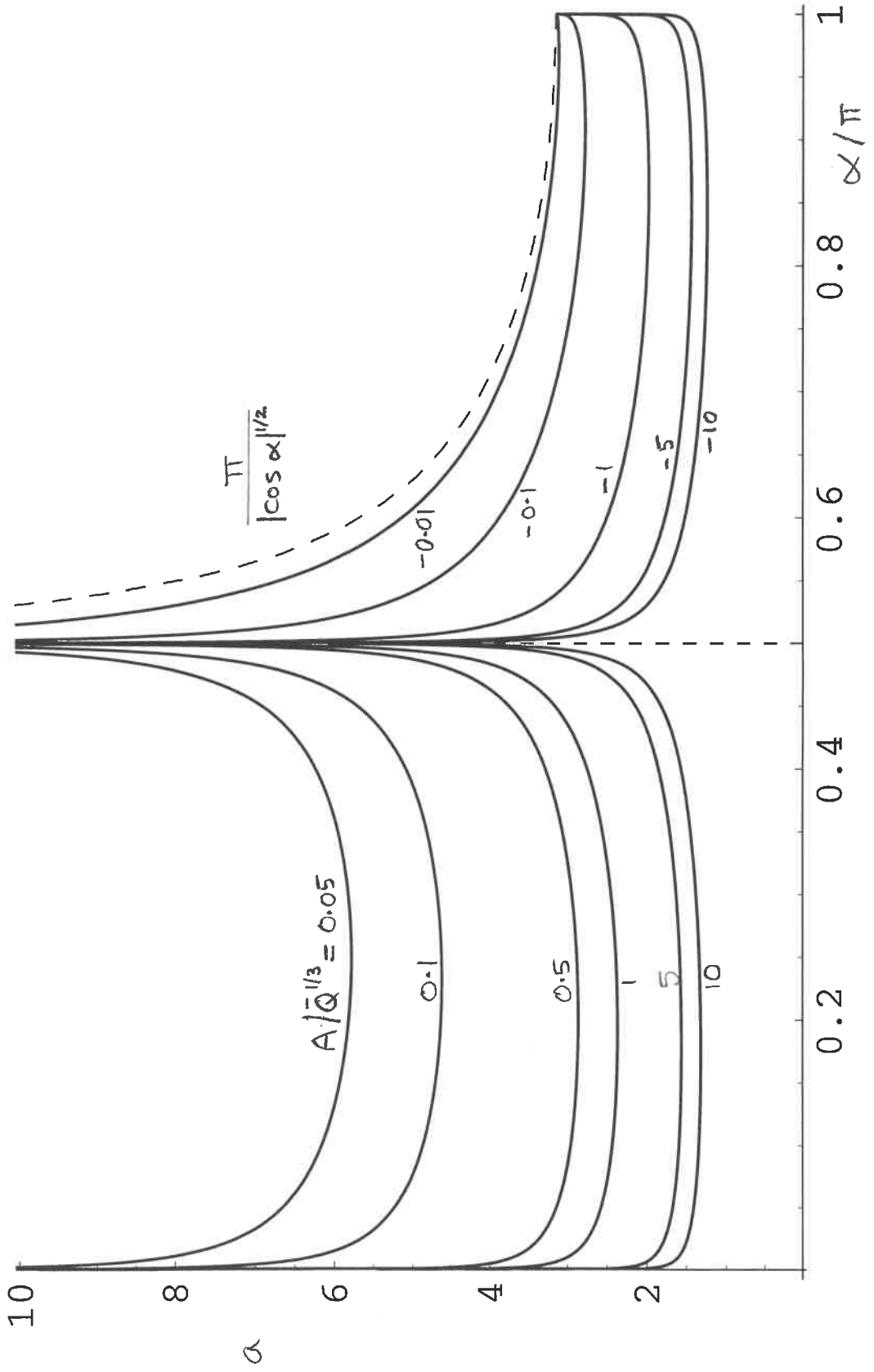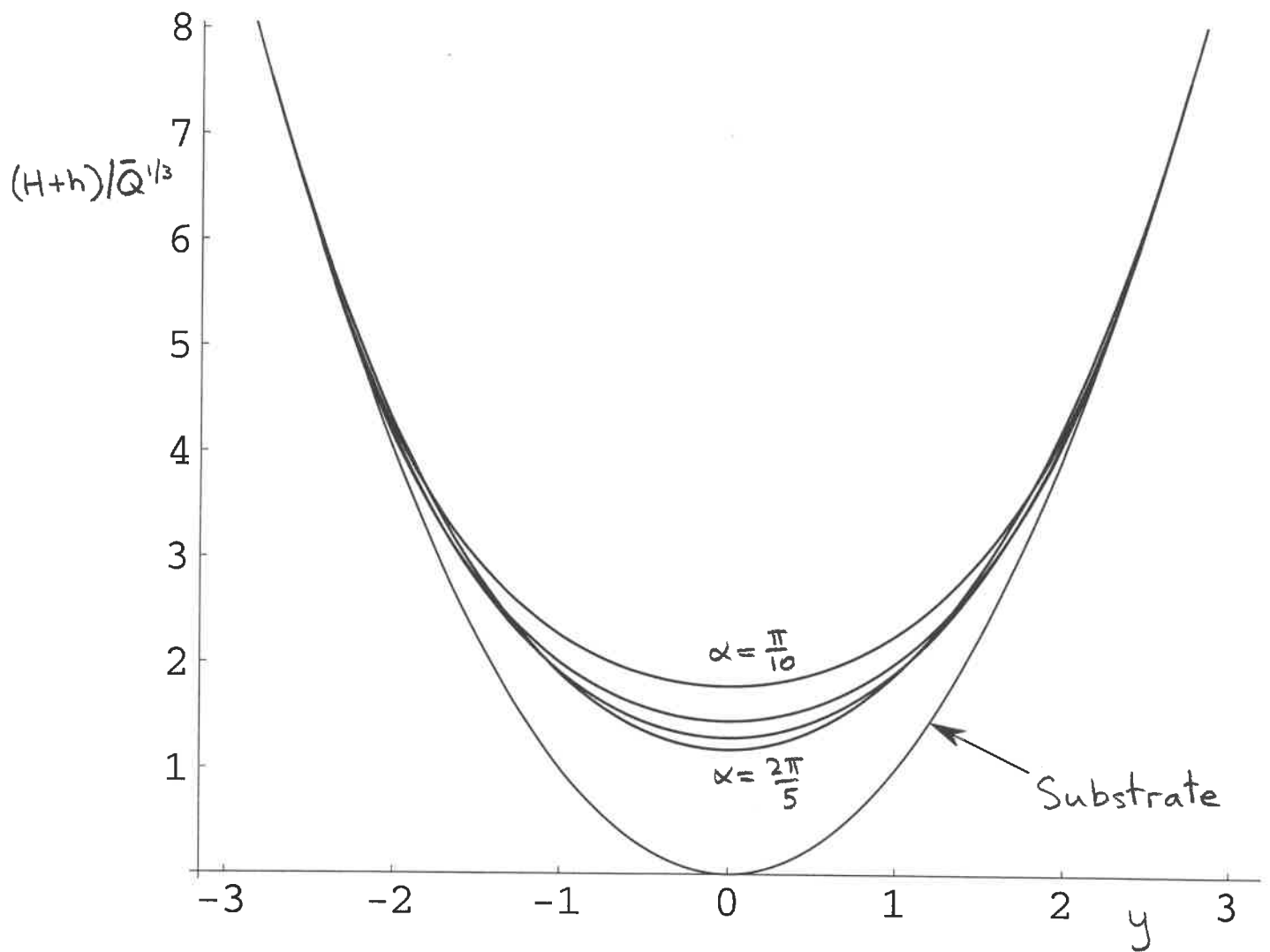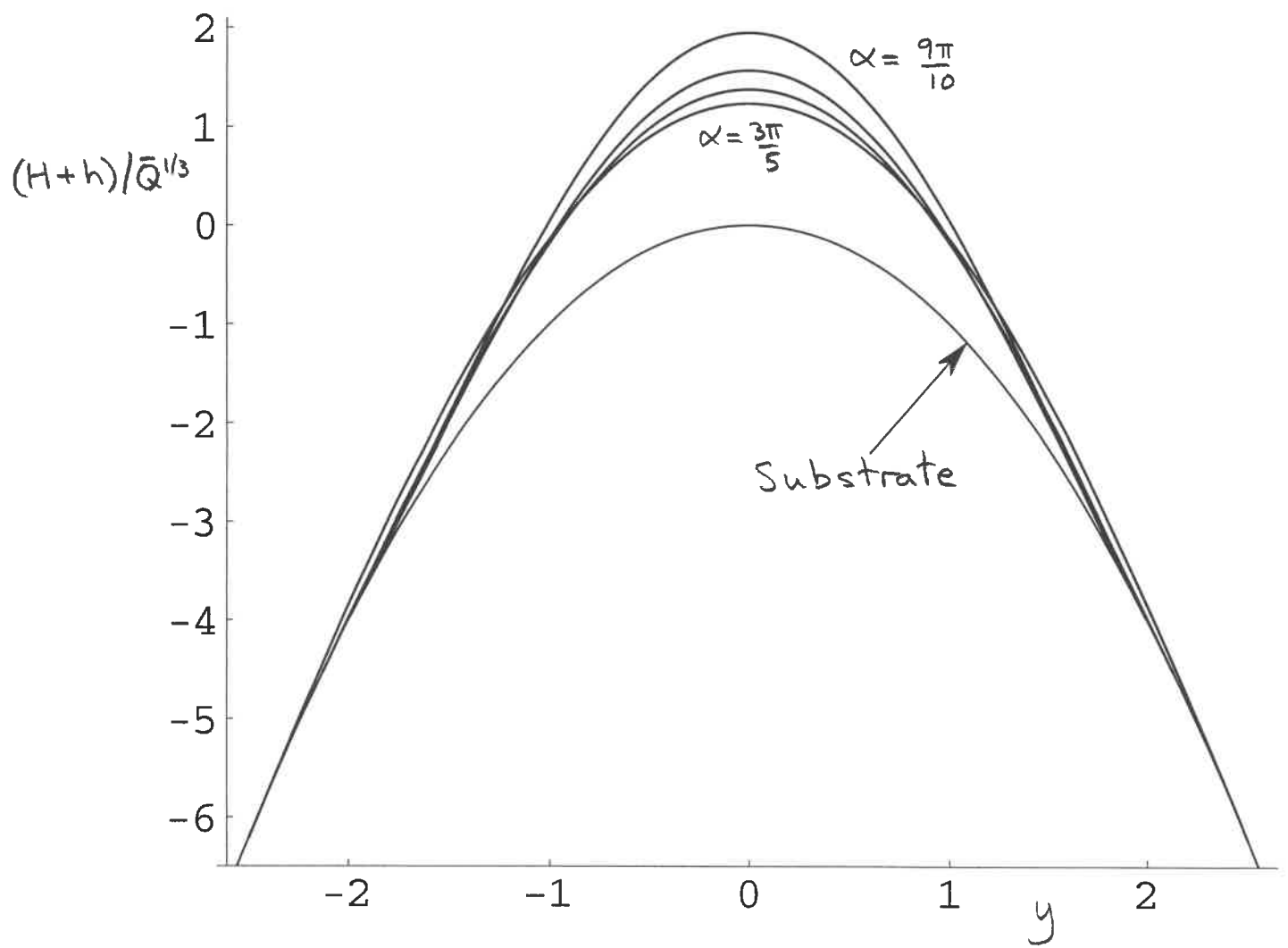
Fig 4(c)

Fig 5(a)

Fig 5(b)

Fig. 6

Fig. 7(a)

Fig. 7(b)

Fig. 8(a)

Fig. 8(b)

Fig. 9(a)

$(H+h)/\bar{Q}^{1/3}$

$\alpha = \dfrac{\pi}{4}$

$\alpha = 0.53\pi$

Substrate

y

Fig. 9(b)

Fig. 10(a)

Fig. 10(b)

$$\frac{\pi}{|\cos \alpha|^{1/2}}$$

$A \cdot |\bar{Q}|^{1/3} = 0.05$

-0.01

-0.1

-1

-5

-10

0.1

0.5

1

5

10

α / π

σ

Fig. 11(a)

$(H+h)/\bar{Q}^{1/3}$

$\alpha = \dfrac{\pi}{10}$

$\alpha = \dfrac{2\pi}{5}$

Substrate

Fig. 11(b)

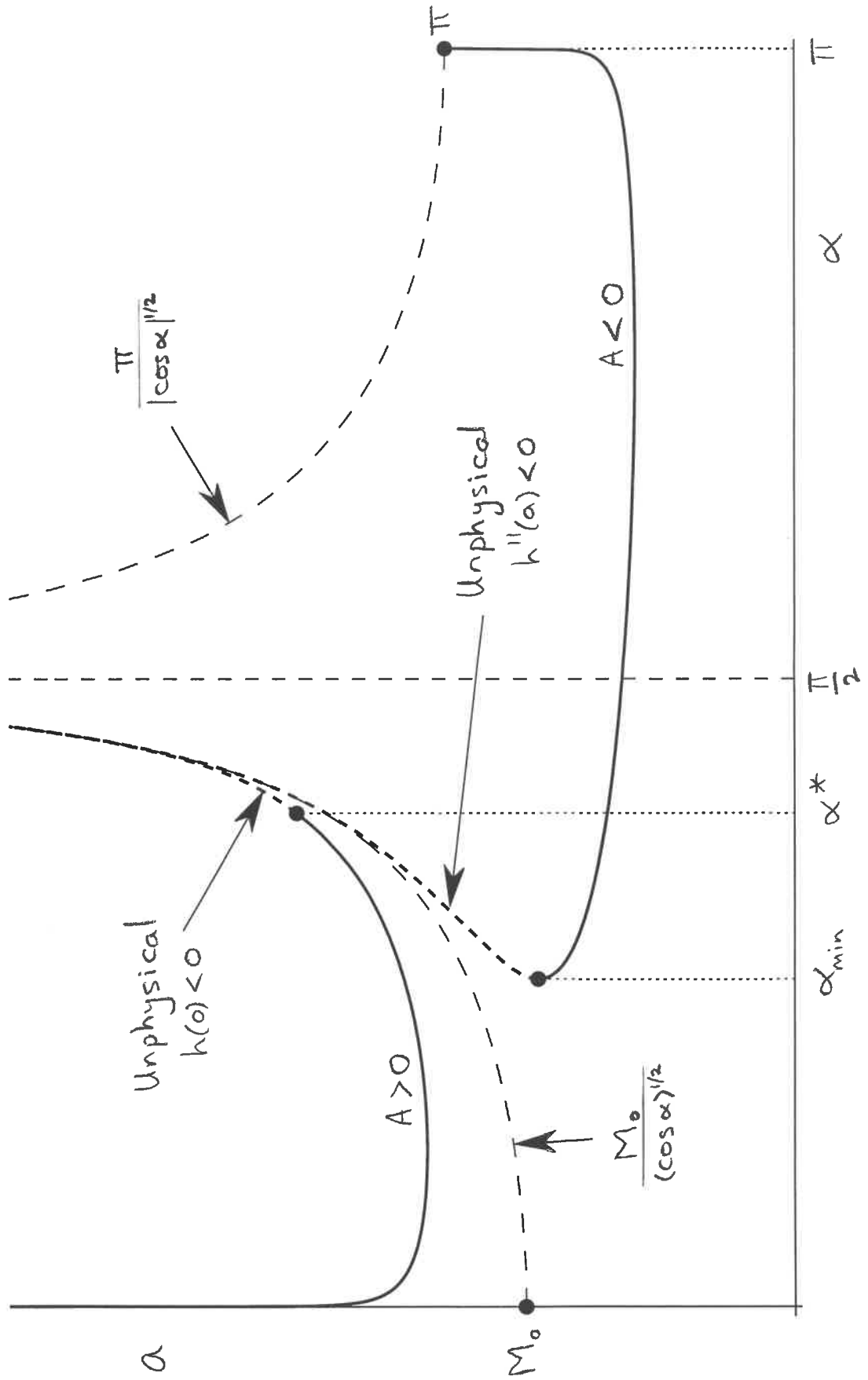$(H+h)/\bar{Q}^{1/3}$

$\alpha = \dfrac{9\pi}{10}$
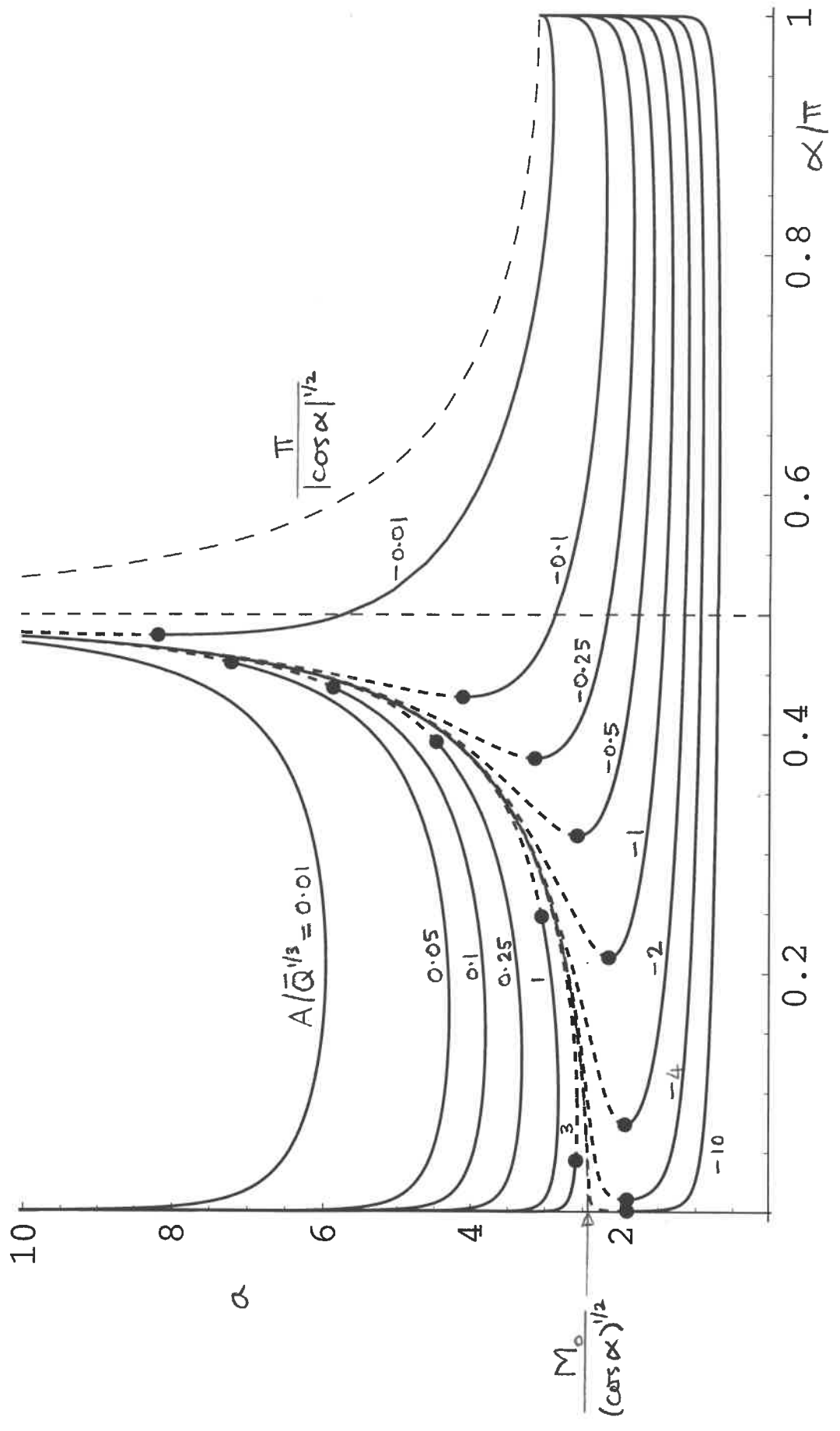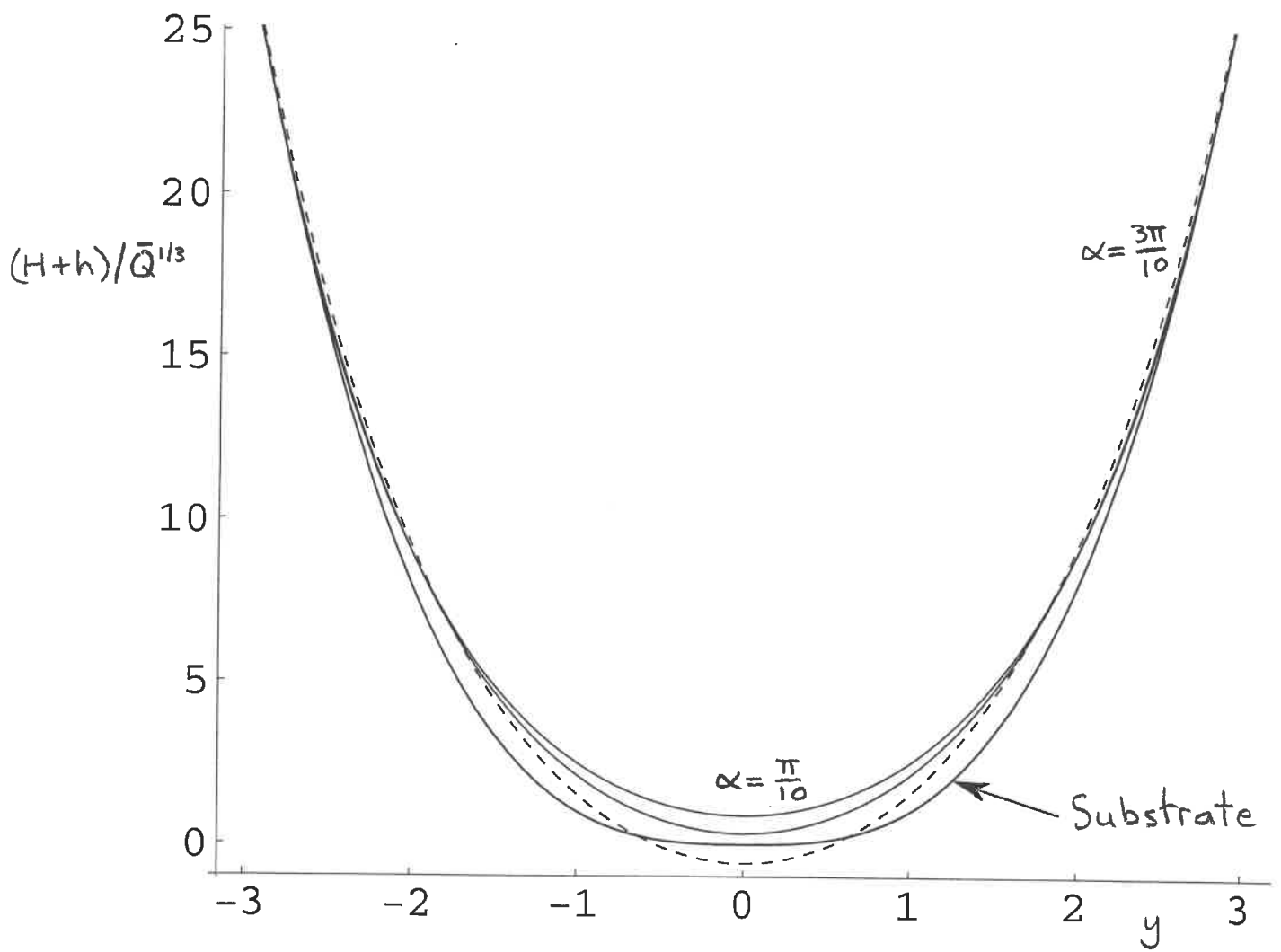
$\alpha = \dfrac{3\pi}{5}$

Substrate

y

Fig. 12(a)

Fig. 12(b)

Fig. 13(a)

Fig. 13(b)

$\alpha = \dfrac{3\pi}{4}$

$\alpha = 0.3\pi$

$(H+h)/\bar{Q}^{1/3}$

Substrate

y